Head and neck cancer cells terminally differentiate reflecting their tissue of origin: a rationale for differentiation therapies

Felix Oppel[1*†], Sarah Gendreizig[1†], Laura Martinez-Ruiz[2-4], Javier Florido[2-4], Alba López-Rodríguez[2-4], Harkiren Pabla[1], Lakshna Loganathan[1], Leonie Hose[1], Philipp Kühnel[1], Pascal Schmidt[5], Matthias Schürmann[1], Judith Martha Neumann[5-6], Flavian Viyof Ful[1], Lars Uwe Scholtz[1], Dina Ligum[7], Frank Brasch[7], Karsten Niehaus[5-6], Germaine Escames[2-4], Tobias Busche[5], Jörn Kalinowski[5], Peter Goon[1], and Holger Sudhoff[1*]

[1] Department of Otolaryngology, Head and Neck Surgery, Campus Klinikum Bielefeld Mitte, University Hospital OWL of Bielefeld University, Teutoburger Str. 50, 33604 Bielefeld, Germany.

[2] Institute of Biotechnology, Biomedical Research Center, Health Sciences Technology Park, University of Granada, Granada, Spain.

[3] Department of Physiology, Faculty of Medicine, University of Granada, 18016 Granada, Spain.

[4] Centro de Investigación Biomédica en Red Fragilidad y Envejecimiento Saludable (CIBERFES), Instituto de Investigación Biosanitaria (Ibs), Granada, San Cecilio University Hospital, Granada, Spain.

[5] Center for Biotechnology (CeBiTec), University Hospital OWL of Bielefeld University, Bielefeld, Germany.

[6] Proteome and Metabolome Research, Faculty of Biology, Bielefeld University, Bielefeld, Germany.

[7] Department of Pathology, Klinikum Bielefeld, Teutoburger Str. 50, 33604, Bielefeld, Germany.

[†] These authors contributed equally to this work

Running title: Head and neck cancer cells terminally differentiate

*** Corresponding author contact:**

Holger Sudhoff, MD, PhD, FRCS (Lon.), FRCPath (Lon.)
Teutoburger Str. 50
33604 Bielefeld, Germany
E-mail: holger.sudhoff@uni-bielefeld.de
tel.: +49 521/581-3301
fax: +49 521/581-3399

Felix Oppel, PhD
Teutoburger Str. 50
33604 Bielefeld, Germany
E-mail: felix.oppel@uni-bielefeld.de
tel.: +49 521/581-3359
fax: +49 521/581-3399

Competing interests: The authors declare no conflict of interest.

Keywords: Head and neck cancer, tumor cell differentiation, cornification

Article metrics: 5905 words, 7 Figures

Abstract

Head and neck squamous cell carcinomas harbor areas of differentiated tissue known as keratin pearls. Using defined cell culture conditions, we modeled this terminal differentiation by cornification in a primary tumor spheroid model leading to increased cell adhesion, proliferation stop, and diminished tumor-initiating potential. RNA-seq, ATAC-seq, and proteome analysis revealed chromatin closure and a wound healing-associated signaling program via STAT3, SMAD2/3, C/EBPβ, c-JUN and other effectors associated with increased expression of KRT17 and cornification markers including SPRR3. Although KRT17 represents a basal stem-cell marker in normal mucosa, we confirm KRT17 as differentiation marker in human HNSCC tissue. Moreover, we describe a common tissue architecture in normal mucosa and HNSCC tissue with distinct cell differentiation states transitioning from a proliferating basal-like compartment to a wound healing-associated signaling zone to a cornifying core. Thus, our data indicate that the targeted differentiation of HNSCC cells may be a promising strategy for anti-HNSCC therapy.

Statement of significance

HNSCC cells can terminally differentiate resembling normal oral mucosa losing their malignancy which indicates therapeutic opportunity.

Introduction

Head and neck squamous cell carcinoma (HNSCC) is a highly malignant disease which represents the 6th most common type of cancer in the world and provides five-year survival rate of about 50% (1,2). Despite recent advances in molecular targeting and immunotherapy the prognosis of affected patients remains devastating. Even though new approaches in immunotherapy and molecular therapy exist, the standard of care for HNSCC remains surgery, cytotoxic chemotherapy, and radiotherapy. These treatments show limited tumor-specificity

and thus frequently damage many vital structures in the head and neck area, leading to a strong morbidity even in long-term survivors (3). Hence, new tumor-specific therapy approaches are urgently needed.

Squamous cell carcinomas are characterized by keratin pearls which are formed by cornifying tumor cells. Cornification represents the normal differentiation path of keratinocytes in the epidermis and the oral mucosa and ensures the formation of a protective barrier on our body`s surface (4). Basal cells in the lowest layer of the skin, called *stratum basale*, are stem cell-like proliferating keratinocytes that constantly renew the epidermis representing the outer protective barrier of human skin (5). The first step in this differentiation process is the exit from the cell cycle and a strengthening of the cells` cytoskeleton in the *stratum spinosum* with a concomitant detachment from the basal membrane. In the next layer, the *stratum granulosum*, keratinocytes acquire a flattened shape of their cell body and nucleus and upregulate keratin and early cornification markers like loricrin and transglutaminase 3 (TGM3) which crosslinks the cytoskeleton to form the cornified envelope. Lipid-filled cellular inclusions called laminar bodies are formed in the cytoplasm. Finally, the *stratum corneum* is formed showing late cornification markers like involucrin and SPRR3. In this stage, the cells gradually lose their organelles and their nucleus and become a dead shell composed of a cornified envelope surrounded by lipid extruded from the lamellar bodies (5). This way stem-like basal cells differentiate, renew the oral mucosa, and thereby create a protective barrier (4).

In the malignant context however, “cell differentiation” is defined by how closely a tumor cell resembles its original tissue, but little is known about the potential of long-term repopulating tumor cells to terminally differentiate and lose their malignancy due to epigenetic changes like chromatin remodeling processes. It is believed that the malignant cell state prevents terminal differentiation (6) or causes a plastic differentiation behavior with mixed or reversible differentiation phenotypes (7-10). Here, we modeled HNSCC cell differentiation, describe differentiation markers, show close similarities in the tissue structure reflecting their normal tissue`s counterpart, and establish initial protocols to trigger this process. This may provide a rational for the development of differentiation therapies driving HNSCC cells into cornification.

Results

HNSCC cornification can be modeled diminishing cell malignancy

The formation of keratin pearls in squamous cell carcinoma tissue is a well-known characteristic of this tumor entity. To study this differentiation process in HNSCC, we employed the primary spheroid model S18 of a previous study (11), further referred as patient 1 (P1). Moreover, we established primary cell culture xenograft tumor model of a second HNSCC patient`s tumor cells (P2; suppl. Table S1). The xenograft tumor resembled the original tumor (suppl. Figure S1A) and adherent cells were isolated from the xenograft tumor tissue that expanded for more than 20 passages in stem cell medium (SCM, suppl. Figure S1B). The cells formed a spindle-like network of adherent cells that released spheroids into the supernatant (Figure 1A, suppl. Figure S1B). After spheroids were harvested from the supernatant, detached, and re-plated into normal flasks, cells regenerated the adherent spheroid-forming cell layer (suppl. Figure S1C), indicating that the spheroid cells as well can repopulate the original cell culture.

A described protocol to interfere with tumor stem cell self-renewal and to induce differentiation is to change from serum-free culture to 10% serum containing Dulbecco′s Modified Eagle′s Medium (DMEM) (9,10,12). Cardiac fibroblast medium (CFM), a medium used to expand primary fibroblasts, had a much stronger differentiating effect than DMEM (Figure 1A). Upon treatment with this medium, P1 cells fully adhered to the culture dish displaying variable but strongly increased cell sizes with pleomorphic cell shapes (Figure 1A) and lost proliferation (Figure 1B). P2 xenograft tumor cells also adhered and acquired enlarged pleomorphic cell bodies (Figure 1A) but continued to proliferate (Figure 1B). CFM cultured cells of P1 developed thickened cell envelopes and cytoplasmic inclusions reminiscent of lamellar bodies, indicative of cornification (Figure 1A). Indeed, we detected about 200x more cornified envelopes in CFM cultured P1 cells than in control cells (Figure 1C). This was insignificant in P2. SCM cultured cells expanded from single cells to whole spheroids/colonies with an efficiency of about 30% which was totally abolished in CFM (Figure 1D). P2 cells were able to efficiently repopulate in

both media, and equally from adherent and spheroid cells in SCM. However, cells in CFM did not form spheroids but grew as adherent colonies, whereas single cell clones of both SCM populations reestablished the mixed adherent/spheroid culture (Figure 1E). Moreover, CFM treatment compromised the survival of P1 and P2 cells (Figure 1F). Transplantation of P1 cells into immunodeficient mice resulted in xenograft tumor formation from SCM cells, whereas in the CFM population tumor-initiating cell (TIC) capacity was annihilated (Figure 1G). In P2, all populations efficiently initiated tumors, but CFM cells displayed delayed tumor onset. SCM-cultured adherent and spheroid cells showed no significant differences. In P1, histopathology analysis also revealed cystic tissue architecture with large areas of necrosis that more closely resembled lymph node metastases than the original tumor (suppl. Figure 2A). For P2, similar cystic tissue architecture of xenograft tumors was observed (suppl. Figure 2B). CFM and SCM tumors matched in histology with insignificantly different extent of tissue cornification (suppl. Figure 2C) indicating that remaining TIC after differentiation treatment retained their imprinted differentiation behavior. P1 tumor tissue displayed small cornified spots with single cell cornification rather than large keratin pearls (suppl. Figure 2). In contrast, P2 tumor tissue was characterized by widespread large cornified patches in primary tumor and xenograft tumors. Altogether, these results show so far that primary HNSCC cells can differentiate by cornification reducing their malignant properties. Within our model, P1 cells appear much more sensitive to our differentiation protocol than those of P2.

HNSCC cell keratinization is associated with chromatin reorganization and wound healing-associated signaling

We performed ATAC-seq, RNA-seq, and global comparative proteome investigations using Nano-LC-ESI MS/MS in our differentiation model to dissect the changes underlying tumor cell differentiation (Figure 2A). ATAC-seq confirmed a reduction of open chromatin regions (OCRs) in the genome upon differentiation by 64.6% in P1 cells and by 59.08% in P2 cells (Figure 2B, suppl. Tables S2), indicating closure of the genome reminiscent of stem cell differentiation in

other systems (13-15). Despite this net loss of chromatin accessibility, the proportion of open small promoters (<1kb) increased 1.75-fold in differentiated P1 cells and 2.05-fold in P2 cells. Larger promoter regions (>1kb) were proportionally not affected (Figure 2C, suppl. Table S3-S5) ATAC-seq showed in both patients that induction of tumor differentiation made OCRs accessible, correlating with epithelial cell differentiation, cell adhesion, and stress-associated pathways which included the regulation of response to wounding, programmed cell death, response to TGF-β, regulation of JNK cascade, and transmembrane receptor tyrosine kinase signaling (Figure 2D, suppl. Tables S6-S7). P2 had no significant response to cytokine stimulus other than P1. Another difference in the two patients' OCRs-related pathways was the RAC1 GTPase cycle signaling determined only in P2.

RNA-seq followed by Gene Ontology (GO) analysis revealed that epithelial differentiation was less intense in P2 compared to P1 cells (Figure 2E-F, suppl. Tables S8-S17). Keratinocyte differentiation, cytoskeleton organization, and keratinization pathways were only upregulated in differentiating P1 cells and not in differentiating P2 cells (Figure 2F). In differentiation medium, cells of P2, but not cells of P1, up-regulated genes mediated to cell migration, cell development, and regulation of signal transduction (Figure 2F).

Transcription factor footprinting (TFF) and Gene Set Enrichment Analysis (GSEA) combining both methods unraveled the mechanisms involved in P1 cell cornification and included TGF-β signaling via R-SMAD proteins SMAD2/3/4, activator protein-1 (AP-1) signaling via c-JUN, JAK/STAT3 signaling, interleukin 6 (IL6) and the pro-inflammatory transcription factor C/EBPβ (Figure 3A-B). GSEA revealed that the TGFβ and JAK/STAT3 pathway genes were highly enriched in the differentiated cancer cells of P1 (Figure 3A). This was not observed in P2 cells. The cornification marker SPRR3 was 9.06-fold more accessible upon differentiation in P1 and upregulated 94.09-fold (suppl. Tables S4 and S8). KRT17 showed 14.59-fold increased accessibility and was upregulated 59.29-fold and displayed a striking accessibility peak only in differentiated P1 cells (Figure 3C). In P2, KRT17 expression increased 2.8-fold (suppl. Table S12). TFF of ATAC-seq data identified p63, c-JUN, C/EBPβ, and SMAD2/3 as transcription factors activated by differentiating conditions in both patients (Figure 3B).

Further, we utilized global expression and proteome data to determine regulatory kinases associated with the differentiation process. RNA-seq identified 24 upregulated and 23 downregulated kinases in differentiating cells of P1. In P2, 23 kinases went up and 13 were downregulated (Figure 3D, suppl. Tables S8-S9 and S12-S13). The global proteome approach specified kinases in the differentiation-medium treated cancer cells of P1 and P2 (Figure 3E, suppl. Tables S18-S25). The receptor tyrosine kinase EPHA2 was identified in differentiation medium-treated cells of both patients from day one until day eight of treatment. This was underlined by the reactome enrichment of the kinases leading to ephrin signaling. The kinase profiling indicates that both cell cultures show signs of cellular senescence during the differentiation treatment and signaling via a TAK1-mediated p38-MAPK, ephrin, JNK, and receptor tyrosine kinases (Figure 3F). This indicates an impact of the MAPK family signaling cascades and the JNK phosphorylation and activation mediated by TAK1 in differentiating HNSCC culture.

Indeed, the OCRs of JNK activation-required MAP-kinases MKK4 and MKK7, which are activated by TAK1 (16), significantly increased 19.27-fold and 5.06-fold upon differentiation of P1 cells (suppl. Table S4) which was not observed in cells of P2. These were also identified in the kinase profiling in differentiated cells of P1 (MKK7 and MKK4, suppl. Tables S18 and S20) and in P2 (MKK4, suppl. Table S22). Overall, three-omics-analysis confirmed the differentiation/keratinization in the P1 model and indicated stress-associated signaling, whereas P2 showed no significant keratinization but signs of epithelial differentiation.

Differentiation-prone signaling is triggered by adhesion

The identified pathways were validated using indirect immunofluorescence (IF). Adherent differentiation medium-treated cells of P1 and P2 displayed nuclear localization of phosphorylation-activated SMAD2 (pSMAD2), C/EBPβ, c-JUN, and pSTAT3 indicating their active signaling which was not observed in spheroid cells of both patients (suppl. Figure S3). Interestingly, adherent undifferentiated cells of P2 displayed strong activation of all four

transcription factors as well, indicating that this active signaling phenotype depended on cell adhesion. When undifferentiated cells were disseminated in differentiation medium with inhibitors of SMAD2/3 (SB525334), JNK (IQ3, upstream of c-JUN), and STAT3 (C188-9), all inhibitors delayed the adhesion of spheroids of P1 (suppl. Figure S4A) which was accompanied by a lower expression of integrin-β1 (ITGB1, suppl. Figure S4B). SMAD2/3, c-JUN, and p-STAT3 were specifically detected in the nuclei of cells at the point of adhesion of differentiating spheroids of P1 (suppl. Figure S4C). P2 cells were not affected phenotypically by the inhibitor treatment. Our data indicate that *in vitro* adhesion was associated with wound healing-associated signaling in HNSCC cells.

High expression of KRT17 and SPRR3 marks HNSCC differentiation

RNA-seq analysis also showed the upregulation of the basal cell-marker KRT17 and small proline-rich proteins like SPRR3 in differentiating P1 cells (suppl. Table S7) which may serve as markers of HNSCC differentiation. IF analysis confirmed a strong upregulation of KRT17 and SPRR3 in CFM-treated P1 cells (Figure 4A). P1 spheroids stained predominantly negative for these markers. In P2, KRT17 was expressed by a subpopulation of cells under any condition, whereas SPRR3 was not detected (Figure 4B). To further investigate KRT17 and SPRR3 as markers of HNSCC differentiation we stained the original patients` tumor tissue which derived P1 and P2 and tissue of four additional patients (P3-6). Normal mucosa attached to the surgically removed tumor piece showed KRT17 expression only in basal cells which was downregulated upon differentiation. SPRR3 initially displayed nuclear localization starting around the middle layer of the stratum spinosum which was then replaced by the formation of an SPRR3+ cell envelope towards the outer mucosal layers (Figure 5B-C). In contrast, KRT17 appeared to precede SPRR3 in HNSCC tissue of all examined patients surrounding keratinized areas, as described previously (17), and to co-localize with SPRR3 towards the core of keratin pearls (Figure 4B-C). This indicates KRT17 as a tumor-specific differentiation marker. P2 and P3 displayed dysplastic tissue adjacent to the tumor. Interestingly, in both

cases KRT17 expression pattern reflected the tumor and not the normal mucosa (Figure 4D) highlighting the reversal of KRT17 from a basal stem cell marker to cornification-associated differentiation-indicating protein to be an early event in HNSCC development.

HNSCC tissue differentiation can be induced by inflammatory mediators

In literature, KRT17 is described to be upregulated in keratinocytes affected by psoriasis, a chronic inflammatory disease mechanistically resembling wound healing (18). Interestingly, psoriasis is driven by the activation of a multitude of signaling pathways and transcription factors including STAT3, C/EBPβ, and AP-1 triggered by damage- or pathogen-associated molecules released from dying keratinocytes and invading inflammatory immune cells. Thus, we investigated whether there is a mechanistic connection between the signaling in psoriasis and HNSCC cornification. In histology, we noticed that keratinization of original tumor tissue of P1 was more intense in lymph node metastases which generally show a more (pseudo-)cystic growth pattern than primary tumors in HNSCC with cysts containing keratin and cellular debris in most cases (19). Interestingly, P1 primary tumor tissue showed only small patches of keratinization, whereas lymph node metastasis tissue displayed larger differentiated areas predominantly surrounding necrotic areas, which was also observed in tumor tissue of other patients (Figure 5A). IF staining revealed expression of cornification marker SPRR3 precisely at the interface between necrotic cysts and the vital tumor tissue (Figure 5B). Thus, we hypothesized that cornification might be triggered by inflammatory signaling from a necrotic possibly immune-invaded environment. In normal skin and psoriasis, cytokines influence the differentiation of keratinocytes (18,20). Thus, we treated P1 cells with described cytokines in SCM. Cytokines like IL1α, IL1β, IL6, IL17A, IL19, IL20, IL22, IL24, TGFβ, Fetuin B (FETUB), oncostatin-M (OSM), and tumor necrosis factor α (TNFα) activated STAT3 signaling and induced a differentiation-like phenotype in HNSCC spheroid cells (Figure 5C). Most effectively, the combination of EGF, IL1α, IL1β, IL6, IL17A, IL22, TGFβ, OSM, and TNFα (CK Mix) induced

adhesion and upregulated expression of adhesion marker ITGB1 and differentiation markers KRT17 and SPRR3 (Figure 5C-D).

HNSCC tissue keratinization resembles normal mucosa differentiation

Above, we describe an *in vitro* model of HNSCC cell differentiation and identified a signaling signature that can be induced by inflammatory cytokines. To verify our results in a larger set of patients, we examined the activity of these pathways utilizing IF in original tumor tissue of P1, P2 and five additional patients (P3-P7) with HNSCC histology (suppl. Table S1, suppl. Figure S5), as well as the xenograft tumor tissue of P1 and P2. This set of HNSCC tissue samples contained cases with intense cornification associated with large keratin pearls (P2-P5, P7) and such with rather single-cell keratinization or small keratin pearls (P1, P6, suppl. Figures S2 and S5). IF staining for c-JUN, C/EBPβ, basal stem-cell marker p63 (21), and proliferation marker Ki67 in combination with the differentiation markers KRT17 and SPRR3 revealed four different zones of marker expression in normal mucosa adjacent to the tumor (Figure 6A-D): 1.) p63+/KRT17+ basal cells showed no activity of any signaling pathway. 2.) Cells in the stratum spinosum directly above the basal layer express Ki67 and p63 but lose KRT17 expression and activate c-JUN and C/EBPβ as evident by nuclear localization of these effectors. About midway in this zone of intense signaling cells start to express SPRR3, initially in nuclear location. 3.) Towards the stratum granulosum SPRR3 changes to cytoplasmic location as part of the cornified envelope. Cell signaling diminishes gradually as cells shut down viable processes during cornification. 4.) In the stratum corneum cells display pyknotic nuclei and stain negative for any marker, presumably due to epitope masking by transglutaminase activity. When we compared this normal mucosa structure to areas on keratinization in HNSCC, we observed that these zones were reflected in the tumor tissue (Figure 6A-D). Tumors with intense cornification showed a zone with small cells at the stroma interface lacking expression of c-JUN and C/EBPβ except Ki67 and p63. The expression of p63 and Ki67 correlated in some patients, whereas in others p63 was expressed throughout

viable cells. In closer proximity to keratin pearls cells become larger with more cytoplasm and nuclei appearing hollow and spotted reminiscent of heterochromatin formation. These cells stain positive for c-JUN and C/EBPβ but lose Ki67 indicating loss of proliferation (Figure 6A-C). KRT17 and SPRR3 are gradually upregulated in this zone. At the interface between this zone and de-stained fully keratinized tumor cells with pyknotic nuclei, frequently cells reside with an irregular morphology and strong SPRR3 expression. However, especially in tissue with low tendency to cornify (P1 and P6) the boundaries of these differentiation zones are difficult to define and the spatial location of cells of each phenotype can be perturbated and chaotic, not organized in sequential layers as normal mucosa and the distinct “layers” may consist of single cells only (Figure 6D). P1 was strongly positive for p63 and Ki67 losing the expression of both markers adjacent to necrotic areas which are prone to differentiation (Figure 6A). Interestingly, P2 cells that do not upregulate SPRR3 and cornify *in vitro* did form tumors in immunodeficient mice that displayed large areas of KRT17+/SPRR3+ keratinization (Figures 4A/6B-C, suppl. Figure S2) indicating that the cells retained their ability to differentiate by cornification. Moreover, increased MKK7 expression correlated with in KRT17 in normal mucosa basal cells and in HNSCC tissue (Figure 6E), indicating a connection between the TAK1-MKK7 axis and KRT17 upregulation in differentiating HNSCC tissue.

In histology of well-differentiated HNSCCs, the four zones described here can also visually be identified (suppl. Figure S6). Thus, altogether we determine that HNSCC cells can undergo terminal differentiation by cornification and mimic the tissue architecture of their normal tissue`s counterpart (Figure 7).

Discussion

HNSCC cells can acquire a truly differentiated state which can be modeled

In this study, we show that HNSCC cells retain the ability to undergo controlled cell death by cornification which represents the path of normal differentiation in oral mucosa. We modeled the transition of undifferentiated tumor-initiating cells to tumor corneocytes which was

accompanied by an overall genome closure similar to stem cell differentiation in other systems (13-15). Our data demonstrate that the state of chromatin accessibility upon tumor differentiation in two patient models was successfully altered, observing a significantly increased proportional accessibility of small promoter regions. This genome closure shows a remodeling process from euchromatin to heterochromatin expansion, described as forming the differentiated state (22,23). We thus demonstrate that HNSCC cells can be forced to differentiate by epigenetic changes in a terminal way losing malignancy, which to our knowledge was only previously shown in neuroblastoma cells upon retinoid-induced ablation of their main oncogenic driver MYCN (24) but not in any type of carcinoma. Moreover, the observation of proportionally increased small promoter accessibility upon tumor cell differentiation has not been reported before and may relate to the ongoing expression housekeeping genes with simple promoters.

It is known that TIC formation and maintenance is controlled epigenetically (25) but little is described about which epigenetic mechanisms allow TICs or cancer stem cells to differentiate into bulk tumor cells. Single-cell RNA-seq revealed the differentiation dynamics of normal stem cells and confirmed that TICs display similar behavior upon transplantation in immunodeficient mice but in a skewed way frequently lacking large parts of normal lineage, displaying plasticity with less discrete differentiation stages, or acquiring irregular phenotypes (7). Compared to single-cell techniques using human tissue, the bulk analysis of our model allows a simultaneous analysis of the malignancy of distinct cell populations. This way, we show a clear loss/reduction of clonal repopulation and tumor-initiating capacity upon forced tumor cell differentiation.

Initiation of HNSCC differentiation activates wound-healing-like signaling

Consistent with the proportional increase of small promoter accessibility, HNSCC cell differentiation *in vitro* directs activation of cell signaling via multiple pathways including but not limited to TGFβ, JNK/AP1, IL-6/JAK/STAT3, and C/EBPβ. In connection to that, we dissected

HNSCC tissue differentiation structure in comparison to normal oral mucosa using indirect immunofluorescence of identified marker proteins of differentiation. We conclude that the basic tissue structure of normal mucosa is reflected in HNSCC with a basal-like stem cell compartment with no differentiation markers, a zone of highly active signaling, and a gradual loss of signaling and differentiation marker positivity in IF staining (Figures 7-8). We identify a signaling program resembling wound healing and psoriasis (18) shared between benign and malignant tissue that includes the activation of c-JUN and C/EBPβ but is much more complex. *In vitro*, TGFβ and STAT3 signaling is also involved but remain to be verified in human tissue.

Remarkably, some of these signaling molecules/pathways are well-described as oncogenic in specific contexts, predominantly c-JUN (26,27), IL-6/JAK/STAT3 (28,29), and TGFβ (30,31). C/EBPβ seems to exert an isoform-specific oncogenic role in breast cancer (32). However, in certain malignancies, these molecules can exert anti-tumor properties in a context-dependent and tumor stage-dependent manner as well. TGFβ is known to function as a tumor suppressor in early-stage tumor development and as an oncogene in later stages (33,34). C/EBPβ can be involved in oncogene-induced senescence (35,36), and c-JUN (37) and STAT3 (38) were implicated in tumor suppressive functions, too. In HNSCC, increased nuclear pSTAT3 was shown to correlate with dismal prognosis (39) and constitutive STAT3 activation is described as an early event in HNSCC development (40). High c-JUN and p-c-JUN expression correlates with poor overall survival in hypopharyngeal squamous cell carcinoma (41). However, the observations in HNSCC indicate an implication of these pathways in tumor biology but do not directly position them in the path from a long-term repopulating HNSCC stem-like cell to a terminally differentiated cell within keratin pearls.

KRT17 is a marker of HNSCC differentiation associated with cornification marker SPRR3

Interestingly, RNA-seq analysis indicated KRT17 to be associated with HNSCC cell differentiation and we observed in various patients` tissue that KRT17 changed from being a basal keratinocyte marker to an early differentiation marker preceding cornification in HNSCC.

KRT17 is described as a stress-associated keratin in the skin and a marker of psoriasis, a chronic wound healing disorder (18). It is plausible that tumor cells upregulate stress-associated signaling as oncogenic genetic alterations cause abnormalities in cell metabolism, protein folding and other vital processes. However, in tumor tissue KRT17 is well-known as an oncoprotein that promotes proliferation, immune evasion, survival, and other malignant hallmarks (42). KRT17 confers increased resistance to cisplatin in cervical cancer (43) and bladder cancer (44) and elevated expression of this gene was described to correlate with poor survival in oropharyngeal squamous cell carcinoma (45). These observations are in stark contrast to our results showing diminished tumor-initiating capacity of differentiated KRT17^{high} cells and an upregulation of this marker in proximity to cornified areas in the HNSCC tissue of distinct patients which is in line with previous reports addressing the spatial expression pattern of KRT17 in HNSCC (17,45). Moreover, high KRT17 expression predicts better survival in HER2^{high} breast cancer (46) and is associated with lower invasion of tumor-promoting regulatory T-cells in HNSCC (47). This indicates a context-dependent role of this marker in tumor biology. In HNSCC, it is also possible that KRT17 is elevated in differentiated HNSCC cells that may not repopulate the tumor but still facilitate onco-promoting functions like drug resistance or metastatic spread. Alternatively, tumors in advanced stages, which should on average have metastasized further than smaller tumors, may contain more differentiated KRT17+ cells due to more widespread necrosis which we observe to be tied to higher differentiation in adjacent HNSCC tissue. This would associate higher malignancy with higher KRT17 levels despite the lack of a causal connection.

Nevertheless, as previously suggested (17,45), our study is the first proving KRT17 as a marker of HNSCC tissue differentiation in association with cornification marker SPRR3. Moreover, our data shows that dysplastic mucosa adjacent to the tumor reflects the tumor`s KRT17 expression pattern with a much stronger abundance of this marker, designating KRT17 as candidate biomarker for HNSCC early detection.

Differentiation in HNSCC and benign mucosa is organized by common tissue layer architecture

Our data show that differentiation in HNSCC and normal mucosa is hierarchically organized with layers of distinct cell populations. The intense activation of signaling via pathways including c-JUN, C/EBPβ, and other pathways thus appears to be the first step in cell differentiation in the benign and malignant context. This is accompanied by a compaction of the genome *in vitro*, and diminished TIC capacity *in vivo*. It is plausible that enlarged cells with a rather condensed genome are less capable to drive tumor disease for long-term, but they may still facilitate oncogenic functions as mentioned above. Thus, the establishment of differentiation therapies in future studies will have to carefully evaluate the impact of this population on tumor biology and how efficient these cells can be driven further into the terminal stage of differentiation.

Moreover, loss of Ki67 expression suggests that cells in the wound healing-associated signaling zone stop proliferation. In well-differentiated tumors we see a basal-like aligned layer of Ki67+/p63+ cells located predominantly at the tumor-stroma interface underneath actively signaling cells downregulating Ki67 and p63 towards the keratin pearl. For P2 this was confirmed in the original tumor and the xenograft tumor showing a remarkable accuracy of the *in vivo* model. P1 displayed an undifferentiated tumor with most cells being p63+/Ki67+ indicating that this tumor was loaded with stem-like cells. It rarely displays small patches of single-cell cornification with a wound healing-associated signaling zone of few cells surrounding SPRR3-positive cells. Thus, the differentiation structure of normal mucosa seems retained in rather undifferentiated tumors as well but presents itself less obvious and more chaotic.

Interestingly, p63 is a known marker of basal stem-cells in the normal skin is essential for proliferation and differentiation of keratinocytes (21) and our data indicate p63 to be a marker of HNSCC stem-like cells, too. It is known that the loss of p63 in normal skin changes the chromatin architecture and enhancer landscape (48-50) which correlates to the reorganization

of the chromatin observed by us during HNSCC cell differentiation associated with decreasing nuclear p63 protein in differentiated areas of HNSCC tissue. Moreover, p63-dependent transcription of epidermal genes in keratinocyte differentiation depends on co-activator transcription factors and the activating epigenetic mark H3K27ac (48,50,51). Thus, p63 is an important regulator of normal keratinocyte differentiation which according to our data might possess a similar role in HNSCC differentiation as well. The underlying mechanisms and co-factors however remain yet largely unknown and should be investigated in future studies.

HNSCC tumor differentiation can be induced by the targeted application of cytokines

Our data indicate that cytokines released by invading immune cells might activate the cornification which represents terminal differentiation and programed cell death of tumor cells. Indeed, using inflammatory cytokines as treatment, we can activate STAT3 and induce adhesion and upregulation of differentiation markers in primary HNSCC cells. Several studies reported that IL6/gp130/STAT3 signaling is associated with the positive regulation of multi-lineage cell differentiation and growth arrest (52-54). This suggests that activators of inflammatory signaling pathways and inhibitors of anti-inflammatory mechanisms in future may serve therapeutic purposes to trigger the differentiation of long-term repopulating cells in HNSCC. This provides a rationale for differentiation therapies in this malignancy proposing an initial protocol.

Differentiation therapies may be more effective in HNSCCs than in other tumor types

In our study we identify distinct HNSCC cell states within the differentiation process which suggests a rather hierarchical organization of long-term tumor repopulation. Tumor-initiating cell dynamics have been investigated previously in colon cancer (COCA) on a functional level. Using clonal marking experiments in serial transplantation in mice, researchers described a hierarchical organization of the colon tumor-initiating cell (TIC) compartment with a subpopulation of long-term repopulating cells and tumor-transiently amplifying cells (T-TACs)

that lost self-renewal capacity and support tumor growth for a limited time frame (55). This well-reflects the organization of normal colon regeneration with self-renewing LGR5+ stem cells at the bottom of the crypts (56) and transiently amplifying cells proliferating for short-term to derive KRT20+ mature gut epithelial cells (57,58). Moreover, another study revealed that colon cancer tissue is structured similar to normal colon with LGR5+ cells residing at the bottom of crypt-like patterns in the tumor tissue that give rise to KRT20+/LGR5- cells (59). However, KRT20+ cells can efficiently repopulate the LGR5+ stem-like compartment upon depletion which demonstrates plasticity between the distinct COCA cell states and that differentiation in COCA is not terminal (8). In another tumor type, pancreatic ductal adenocarcinoma (PDAC), we previously observed as well that long-term tissue repopulation was similar in benign and malignant tissue with a clonal succession of transient TICs (9), reflecting the transient de-differentiation of acinar cells to regenerate defects in the normal exocrine pancreas (60). Thus, COCA and PDAC TICs display plasticity in their phenotypic and functional differentiation which is believed to be a general phenomenon allowing tumors to avoid terminal differentiation by epigenetic mechanisms (25). This might interfere with therapeutic ambitions to drive TIC into terminal differentiation associated with an irreversible loss of self-renewal. In contrast, our HNSCC differentiation model leads to cornification, which is terminal, and loss of malignant behavior, so differentiation therapies may be more efficient in this neoplasm than in other cancer types, which should be established in following studies.

Conclusions

Altogether, we dissected the terminal differentiation of HNSCC cells, modeled this process, relate it to lower malignancy, describe associated markers like KRT17, demonstrate that cytokine treatment is sufficient to induce a differentiation phenotype, and describe the spatial location of distinct cell populations in human tissue. However, a limitation of our study is that we did not yet identify one targetable mechanism or molecule that controls the epigenetic transition from a malignant cell to an irreversibly differentiated cell. It seemed to us that every

new knot unraveled opens another magnitude of complexity in the dynamics and regulation of HNSCC differentiation and multiple future studies will be necessary to fully understand every aspect of this process.

Material and Methods

Human material and cell culture

Primary head and neck cancer tissue was obtained from medically indicated surgeries with informed consent of the patients, according to the declaration of Helsinki, and as approved by the ethics committee of the Ruhr-University Bochum (AZ 2018-397_3). The cells were cultured in PneumaCult™-Ex Plus Medium, referred as stem cell medium (SCM, #05041, Stemcell Technologies, Vancouver, Canada) supplemented as described previously (11). Adherent cells and spheroids were detached using Accutase (Capricorn Scientific, Ebsdorfergrund, Germany). Cells were differentiated in cardiac fibroblast medium (CFM, 316K-500, Cell Applications, San Diego, CA, United States) supplemented with 1% 200 mM L-Glutamine, 1% 100x Penicillin/Streptomycin, and 1% 250 µg/mL Amphotericin B solution (all three Capricorn Scientific). Dulbecco's Modified Eagle Medium (DMEM, DMEM-HXA, Capricorn Scientific) was supplemented with 10% Fetal Bovine Serum Advanced (FBS Advanced, FBS-11A, Capricorn Scientific), L-Glutamine, Penicillin/Streptomycin, and Amphotericin B. Cells received fresh medium twice a week. Cells were analyzed for proliferation, cornification, and treated with drugs and cytokines as outlined in supplementary methods.

Mouse xenograft tumor models

All animal experiments were conducted as approved by the Institutional Animal Care and Use Committee of the University of Granada (procedures 12/07/2019/128) in accordance with the European Convention for the Protection of Vertebrate Animals used for Experimental and Other Scientific Purposes (CETS #123) and Spanish law (R.D. 53/2013).

NSG mice (NOD.Cg-Prkdcscid Il2rgtm1Wjl/SzJ, The Jackson Laboratory, Bar Harbor, ME, United States) were housed in appropriate sterile filter-capped cages with sterile food and water ad libitum. $1x10^6$ cells were transplanted subcutaneously into the left and right flank of each mouse as described previously (61), with differentiated and undifferentiated cell populations being injected side-by-side as performed in a previous study (9). Animals were monitored for tumor development twice a week. Tumor sizes were measured using a vernier caliper and tumor volume was calculated by the formula (width×length2)/2. When the first tumor of each population reached the legal size limit, all mice of that experiment were measured and sacrificed. Tumors were harvested and fixed in 4% paraformaldehyde (PFA, 2.529.311.214, PanReac) for 24 hours. The fixed samples were embedded in paraffin following standard protocols.

Histopathology analysis of HNSCC tissue

Paraffin-embedded tissue was sectioned with 2 µm thickness using a sliding HM430 microtome (Zeiss). Hematoxylin/Eosin (HE) staining was performed using standard protocols in a linear COT 20 tissue stainer (MEDITE, Burgdorf, Germany). HE stained section were analyze by a senior pathologist (F.B.) to compare patient characteristics between original tumor and xenograft tumor models. To quantify keratinized areas in human tumor tissue every HE-stained section was subdivided into three random views and analyzed using an Axio Lab.1 microscope (Zeiss) and DISKUS software (Hilgers, Königswinter, Germany). Per view, the total area displaying malignant histology was determined in mm^2. Next, the keratinized area within the tumor compartment was determined to calculate the proportional extent of cornification using Microsoft Excel.

Indirect Immunofluorescence of HNSCC cells and tissue

Indirect Immunofluorescence (IF) of HNSCC cell cultures was performed as described previously (62). Tumor tissue of patients and xenograft tumor models was analyzed by IF as

established in prior studies (9,63). Samples were imaged using a LSM780 confocal microscope (Zeiss, Oberkochen, Germany) and ZEN software (Zeiss). Primary antibodies: mouse-anti-human C/EBPβ (1:100, H-7, sc-7962), mouse-anti-human c-JUN (1:100, G-4, sc-74543), mouse-anti-human esophagin (SPRR3, 1:100, E-6, sc-514844), mouse-anti-human KRT17 (1:100, E-4, sc-393002), mouse-anti-human MEK-7 (MKK7, 1:100, E-7, sc-25288), mouse-anti-human p63 (1:100, D-9, sc-25268), mouse-anti-human SMAD2/3 (1:100, A-3, sc-398844, all Santa Cruz Biotechology, Dallas, TX, United States), rabbit-anti-human Ki67 (1:200, SP6, ab16667, Abcam), rabbit-anti-human SPRR3 (1:200, NBP2-13374, Novus Biologicals/Bio-Techne, Abingdon, United Kingdom), rabbit-anti-human phospho-STAT3-Y705 (1:200, A16431, Antibodies Online, Aachen, Germany), rabbit-anti-human phospho-SMAD2-S465/S467 (1:50, E8F3R, 18338T, Cell Signaling Technologies), and guinea pig-anti-human KRT17; secondary antibodies: goat-anti-mouse-IgG-Alexa Fluor-555 (1:400, A21422), donkey-anti-rabbit-IgG-Alexa Fluor-488 (1:400, A11008), and goat-anti-guinea pig-IgG-Alexa Fluor-647 (1:400, A21450, all Thermo Fisher Scientific, Waltham, MA, United States). DNA was stained with DAPI (Sigma Aldrich, St. Louis, MO, United States) using 2µg/ml diluted in PBS + 0.1% bovine serum albumin (Capricorn Scientific).

RNA isolation and real-time quantitative PCR

Total RNA was isolated from cultured cells using innuPREP DNA/RNA Mini Kit (Analytik Jena, Jena, Germany) as recommended by the manufacturer's protocol. RNA quality was determined with a BioDrop Duo+ spectral photometer (Biochrom, Holliston, USA). Real-time quantitative PCR (RT-qPCR) was conducted as described previously (11) using the following primers:

GAPDH-forward: CTGCACCACCAACTGCTTAG,

GAPDH-reverse: GTCTTCTGGGTGGCAGTGAT,

ITGB1-forward: GACGCCGCGCGGAAAAG,

ITGB1-reverse: TCTGGAGGGCAACCCTTCTT,

KRT17-forward: CCTCAATGACCAACACTGAGC,

KRT17-reverse: GTCTCAAACTTGGTGCGGAA,

SPRR3-forward: TGCACAGCAGGTCCAGCA,

SPRR3-reverse: GGCTCCTTGGTTGTGGGAA.

Multi-omics analysis of HNSCC cell differentiation

Differentiated and undifferentiated HNSCC cell populations were examined by RNA-seq, ATAC-seq, and Nano-LC-ESI MS/MS analysis as outlined in supplementary methods.

Single cell cloning assay

Cells were detached and seeded into U-bottom 96-wells at a density of approximately 1 cell/well in 100 µl volume of the desired medium. Plates were centrifuged and all wells were examined in a light microscope (Leica, Wetzlar, Germany) to identify wells containing single cells. These wells were reexamined after 5, 14, and 21 days to monitor proliferation behavior of single-cell clones. Cells received fresh medium once a week. Obtained data was processed in Microsoft Excel (Microsoft Corporation, Redmond, WA, United States) and visualized using GraphPad Prism software (Graphpad Software Inc., San Diego, CA, United States).

Figures

Figure 1

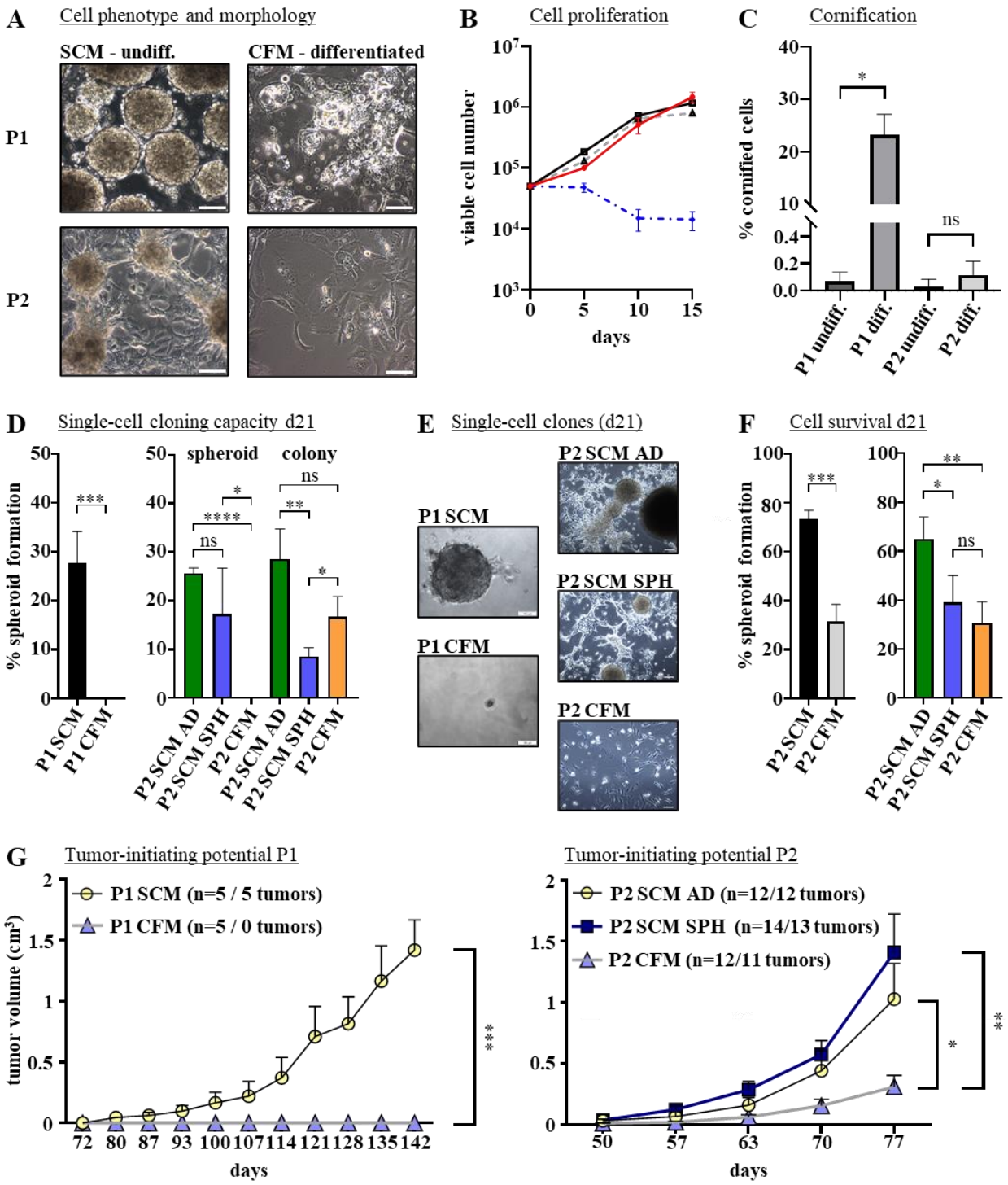

Figure 2

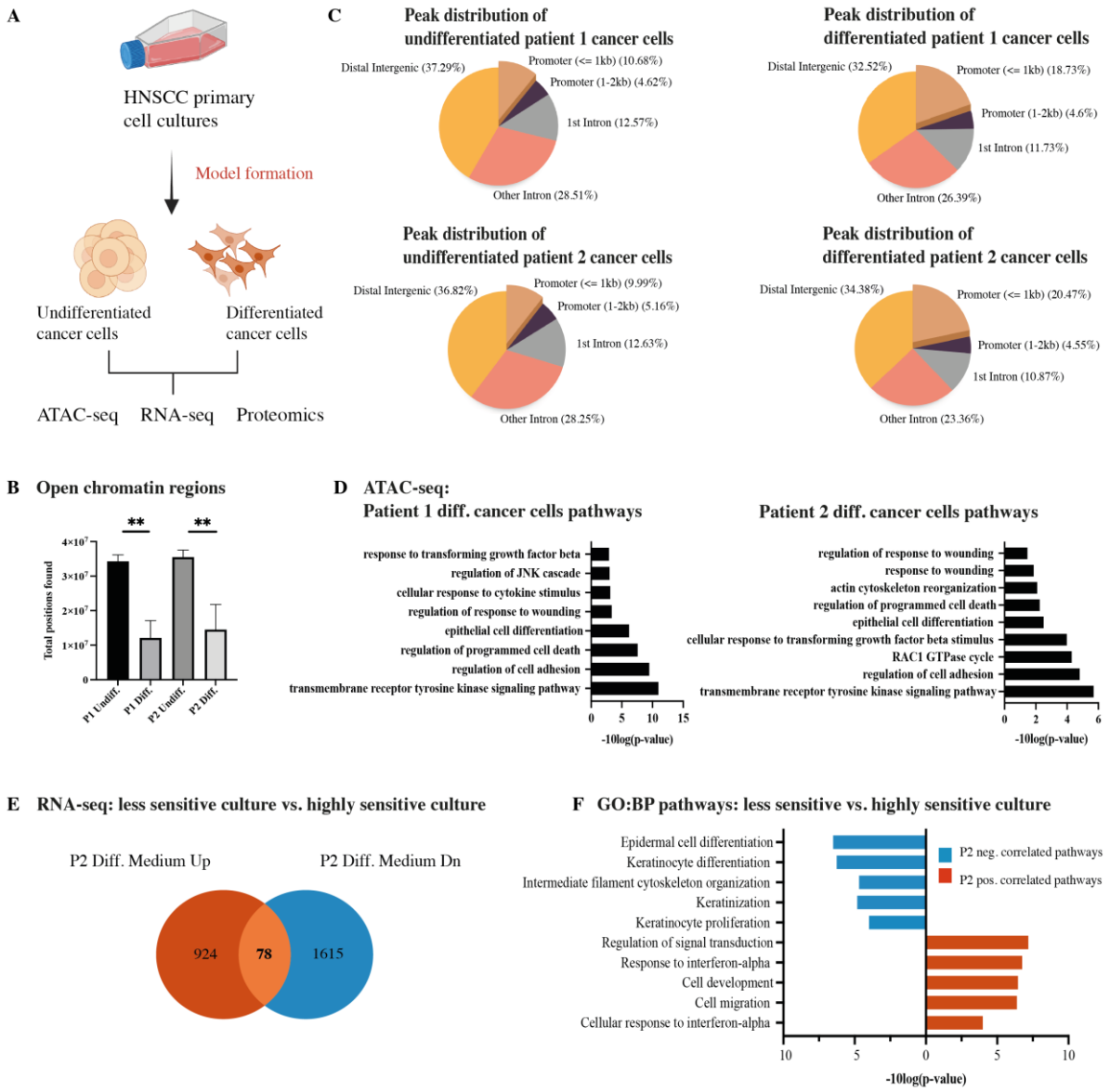
A
HNSCC primary cell cultures
Model formation
Undifferentiated cancer cells
Differentiated cancer cells
ATAC-seq
RNA-seq
Proteomics
C
Peak distribution of undifferentiated patient 1 cancer cells
Distal Intergenic (37.29%)
Promoter (<= 1kb) (10.68%)
Promoter (1-2kb) (4.62%)
1st Intron (12.57%)
Other Intron (28.51%)
Peak distribution of differentiated patient 1 cancer cells
Distal Intergenic (32.52%)
Promoter (<= 1kb) (18.73%)
Promoter (1-2kb) (4.6%)
1st Intron (11.73%)
Other Intron (26.39%)
Peak distribution of undifferentiated patient 2 cancer cells
Distal Intergenic (36.82%)
Promoter (<= 1kb) (9.99%)
Promoter (1-2kb) (5.16%)
1st Intron (12.63%)
Other Intron (28.25%)
Peak distribution of differentiated patient 2 cancer cells
Distal Intergenic (34.38%)
Promoter (<= 1kb) (20.47%)
Promoter (1-2kb) (4.55%)
1st Intron (10.87%)
Other Intron (23.36%)
B Open chromatin regions
Total positions found
P1 Undiff.
P1 Diff.
P2 Undiff.
P2 Diff.
D ATAC-seq:
Patient 1 diff. cancer cells pathways
response to transforming growth factor beta
regulation of JNK cascade
cellular response to cytokine stimulus
regulation of response to wounding
epithelial cell differentiation
regulation of programmed cell death
regulation of cell adhesion
transmembrane receptor tyrosine kinase signaling pathway
-10log(p-value)
Patient 2 diff. cancer cells pathways
regulation of response to wounding
response to wounding
actin cytoskeleton reorganization
regulation of programmed cell death
epithelial cell differentiation
cellular response to transforming growth factor beta stimulus
RAC1 GTPase cycle
regulation of cell adhesion
transmembrane receptor tyrosine kinase signaling pathway
-10log(p-value)
E RNA-seq: less sensitive culture vs. highly sensitive culture
P2 Diff. Medium Up
P2 Diff. Medium Dn
924
78
1615
F GO:BP pathways: less sensitive vs. highly sensitive culture
Epidermal cell differentiation
Keratinocyte differentiation
Intermediate filament cytoskeleton organization
Keratinization
Keratinocyte proliferation
Regulation of signal transduction
Response to interferon-alpha
Cell development
Cell migration
Cellular response to interferon-alpha
P2 neg. correlated pathways
P2 pos. correlated pathways
-10log(p-value)

Figure 3

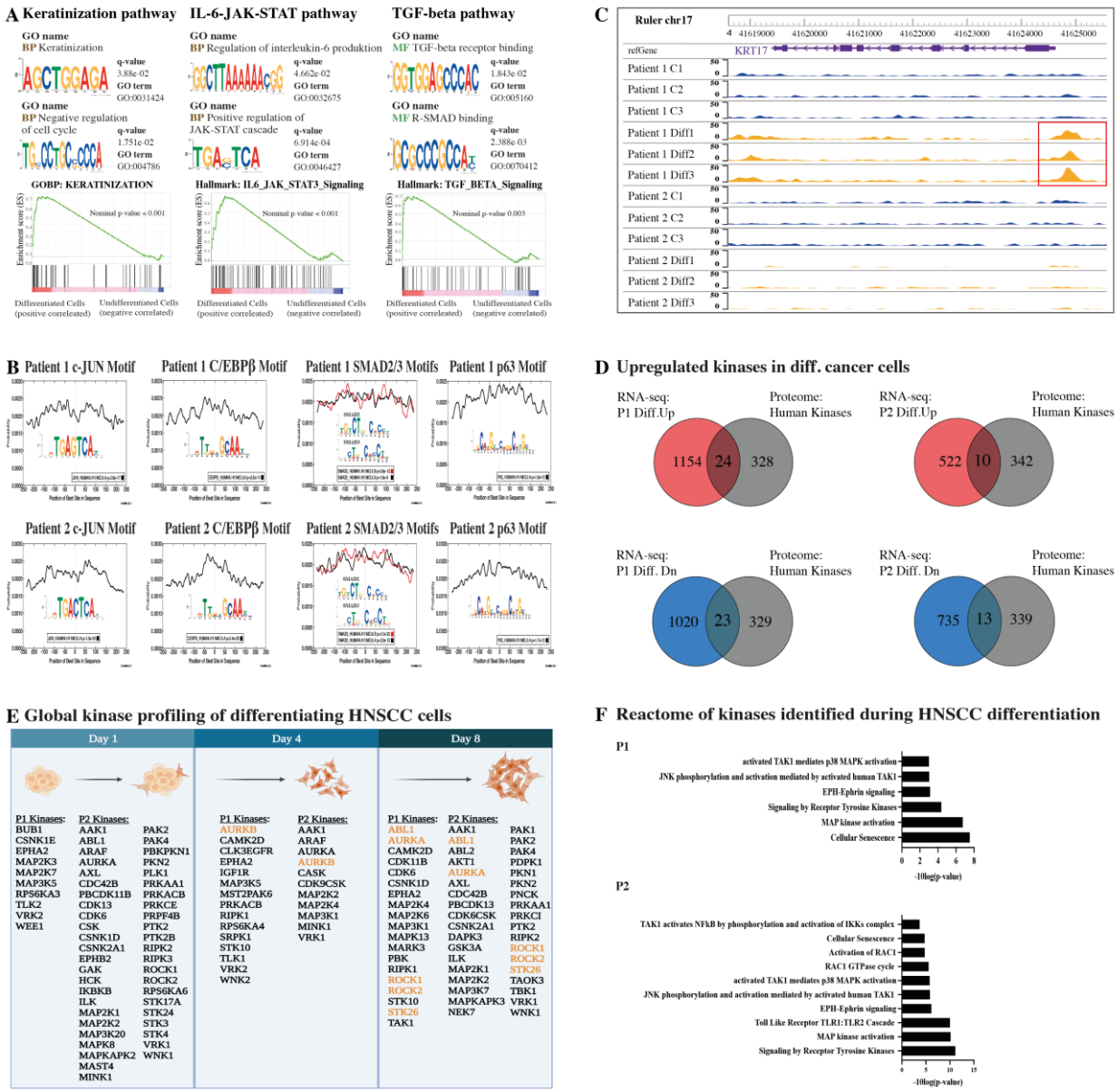
A Keratinization pathway
IL-6-JAK-STAT pathway
TGF-beta pathway
GO name
BP Keratinization
q-value
3.88e-02
GO term
GO:0031424
GO name
BP Negative regulation of cell cycle
q-value
1.751e-02
GO term
GO:004786
GO name
BP Regulation of interleukin-6 produktion
q-value
4.662e-02
GO term
GO:0032675
GO name
BP Positive regulation of JAK-STAT cascade
q-value
6.914e-04
GO term
GO:0046427
GO name
MF TGF-beta receptor binding
q-value
1.843e-02
GO term
GO:005160
GO name
MF R-SMAD binding
q-value
2.388e-03
GO term
GO:0070412
GOBP: KERATINIZATION
Hallmark: IL6_JAK_STAT3_Signaling
Hallmark: TGF_BETA_Signaling
Nominal p-value < 0.001
Nominal p-value < 0.001
Nominal p-value 0.003
Enrichment score (ES)
Differentiated Cells (positive correleated)
Undifferentiated Cells (negative correlated)
C
Ruler chr17
refGene
KRT17
Patient 1 C1
Patient 1 C2
Patient 1 C3
Patient 1 Diff1
Patient 1 Diff2
Patient 1 Diff3
Patient 2 C1
Patient 2 C2
Patient 2 C3
Patient 2 Diff1
Patient 2 Diff2
Patient 2 Diff3
B Patient 1 c-JUN Motif
Patient 1 C/EBPβ Motif
Patient 1 SMAD2/3 Motifs
Patient 1 p63 Motif
Patient 2 c-JUN Motif
Patient 2 C/EBPβ Motif
Patient 2 SMAD2/3 Motifs
Patient 2 p63 Motif
D Upregulated kinases in diff. cancer cells
RNA-seq: P1 Diff.Up
Proteome: Human Kinases
1154
24
328
RNA-seq: P2 Diff.Up
Proteome: Human Kinases
522
10
342
RNA-seq: P1 Diff. Dn
Proteome: Human Kinases
1020
23
329
RNA-seq: P2 Diff. Dn
Proteome: Human Kinases
735
13
339
E Global kinase profiling of differentiating HNSCC cells
Day 1
Day 4
Day 8
P1 Kinases:
BUB1
CSNK1E
EPHA2
MAP2K3
MAP2K7
MAP3K5
RPS6KA3
TLK2
VRK2
WEE1
P2 Kinases:
AAK1
ABL1
ARAF
AURKA
AXL
CDC42B
PBCDK11B
CDK13
CDK6
CSK
CSNK1D
CSNK2A1
EPHB2
GAK
HCK
IKBKB
ILK
MAP2K1
MAP2K2
MAP3K20
MAPK8
MAPKAPK2
MAST4
MINK1
PAK2
PAK4
PBKPKN1
PKN2
PLK1
PRKAA1
PRKACB
PRKCE
PRPF4B
PTK2
PTK2B
RIPK2
RIPK3
ROCK1
ROCK2
RPS6KA6
STK17A
STK24
STK3
STK4
VRK1
WNK1
P1 Kinases:
AURKB
CAMK2D
CLK3EGFR
EPHA2
IGF1R
MAP3K5
MST2PAK6
PRKACB
RIPK1
RPS6KA4
SRPK1
STK10
TLK1
VRK2
WNK2
P2 Kinases:
AAK1
ARAF
AURKA
AURKB
CASK
CDK9CSK
MAP2K2
MAP2K4
MAP3K1
MINK1
VRK1
P1 Kinases:
ABL1
AURKA
CAMK2D
CDK11B
CDK6
CSNK1D
EPHA2
MAP2K4
MAP2K6
MAP3K1
MAP3K13
MARK3
PBK
RIPK1
ROCK1
ROCK2
STK10
STK26
TAK1
P2 Kinases:
AAK1
ABL1
ABL2
AKT1
AURKA
AXL
CDC42B
PBCDK13
CDK6CSK
CSNK2A1
DAPK3
GSK3A
ILK
MAP2K1
MAP2K2
MAP3K7
MAPKAPK3
NEK7
PAK1
PAK2
PAK4
PDPK1
PKN1
PKN2
PNCK
PRKAA1
PRKCI
PTK2
RIPK2
ROCK1
ROCK2
STK26
TAOK3
TBK1
VRK1
WNK1
F Reactome of kinases identified during HNSCC differentiation
P1
activated TAK1 mediates p38 MAPK activation
JNK phosphorylation and activation mediated by activated human TAK1
EPH-Ephrin signaling
Signaling by Receptor Tyrosine Kinases
MAP kinase activation
Cellular Senescence
-10log(p-value)
P2
TAK1 activates NFkB by phosphorylation and activation of IKKs complex
Cellular Senescence
Activation of RAC1
RAC1 GTPase cycle
activated TAK1 mediates p38 MAPK activation
JNK phosphorylation and activation mediated by activated human TAK1
EPH-Ephrin signaling
Toll Like Receptor TLR1:TLR2 Cascade
MAP kinase activation
Signaling by Receptor Tyrosine Kinases
-10log(p-value)

Figure 4

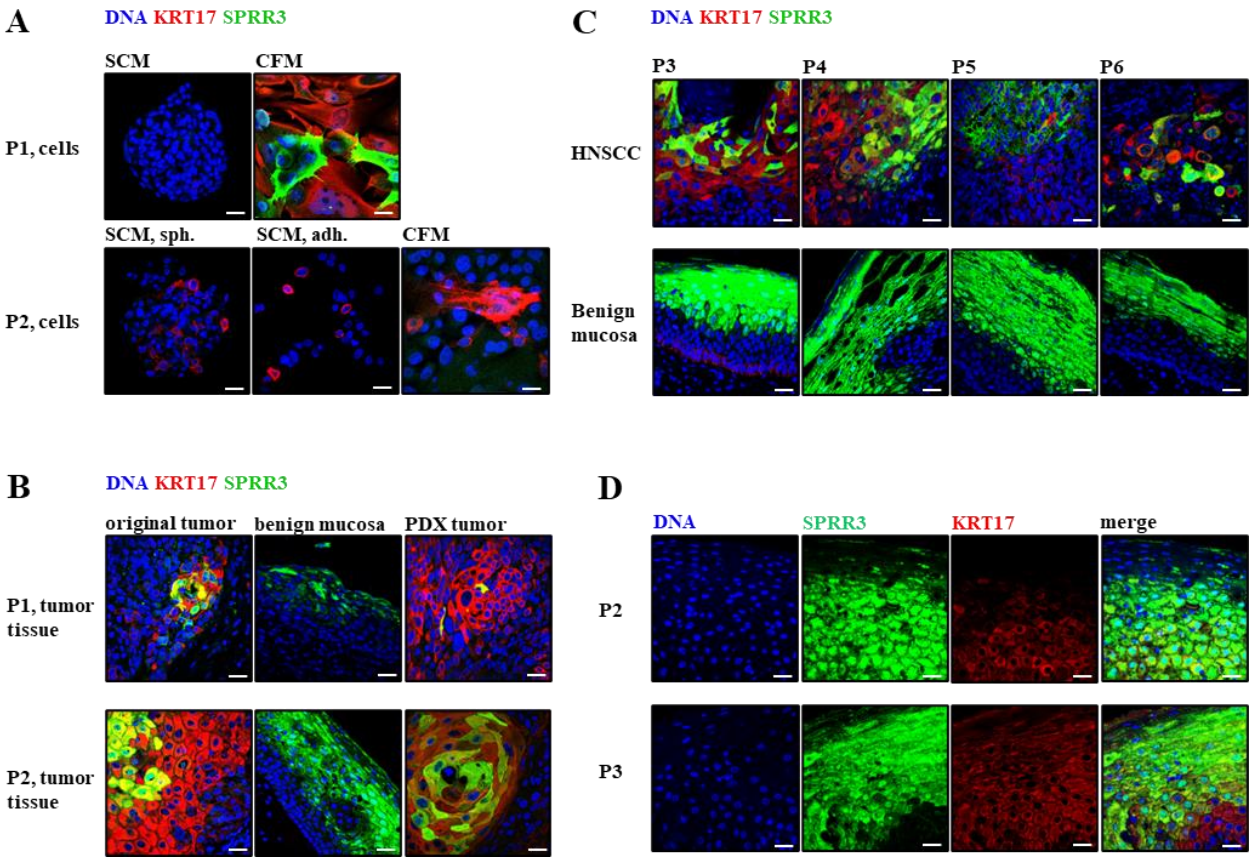
A
DNA KRT17 SPRR3
SCM
CFM
P1, cells
SCM, sph.
SCM, adh.
CFM
P2, cells
C
DNA KRT17 SPRR3
P3
P4
P5
P6
HNSCC
Benign mucosa
B
DNA KRT17 SPRR3
original tumor
benign mucosa
PDX tumor
P1, tumor tissue
P2, tumor tissue
D
DNA
SPRR3
KRT17
merge
P2
P3

Figure 5

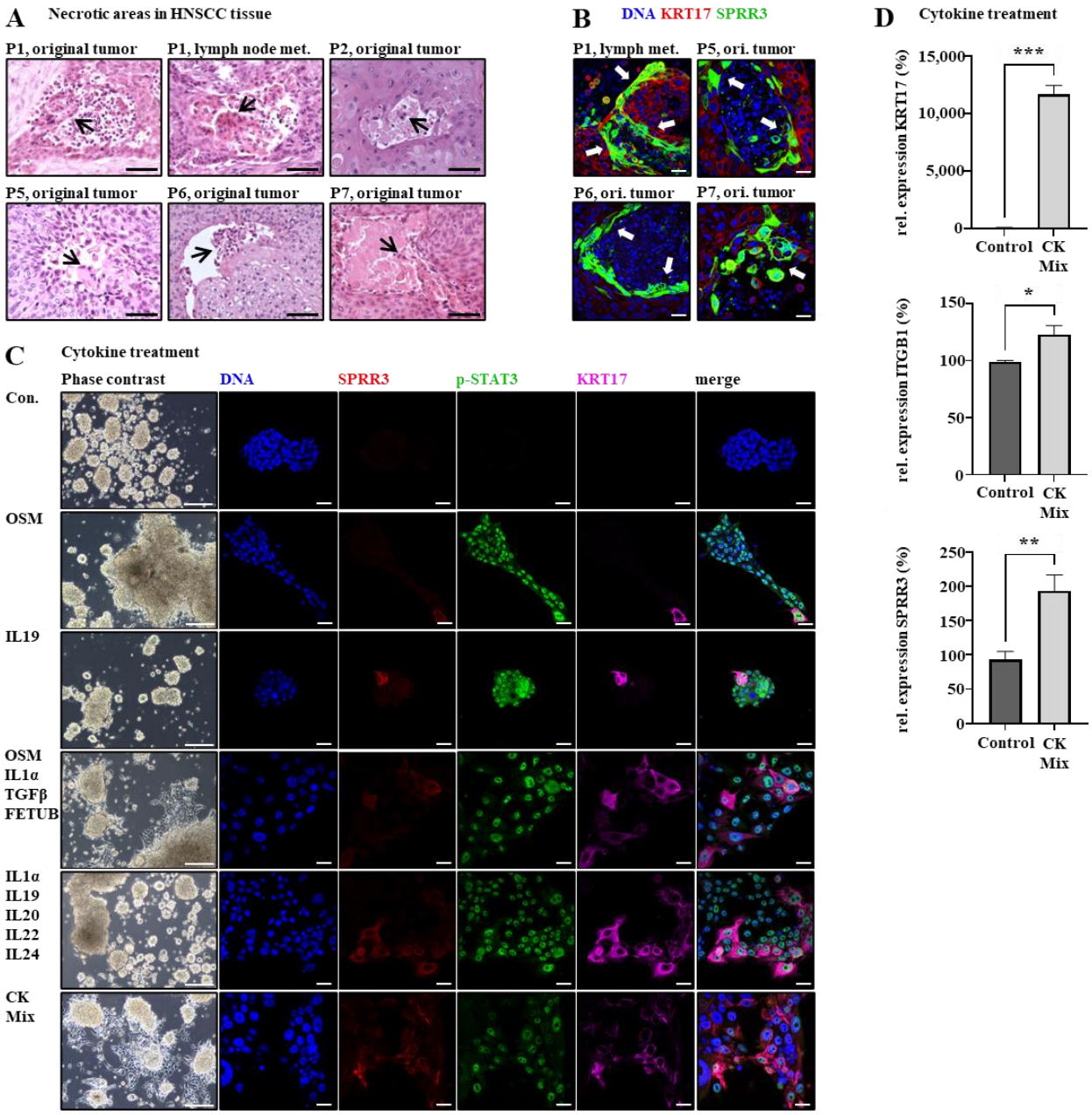
A
Necrotic areas in HNSCC tissue
P1, original tumor
P1, lymph node met.
P2, original tumor
P5, original tumor
P6, original tumor
P7, original tumor
B
DNA KRT17 SPRR3
P1, lymph met.
P5, ori. tumor
P6, ori. tumor
P7, ori. tumor
C
Cytokine treatment
Phase contrast
DNA
SPRR3
p-STAT3
KRT17
merge
Con.
OSM
IL19
OSM
IL1α
TGFβ
FETUB
IL1α
IL19
IL20
IL22
IL24
CK
Mix
D
Cytokine treatment
rel. expression KRT17 (%)
15,000
10,000
5,000
0
***
Control
CK Mix
rel. expression ITGB1 (%)
150
100
50
0
*
Control
CK Mix
rel. expression SPRR3 (%)
250
200
150
100
50
0
**
Control
CK Mix

Figure 6

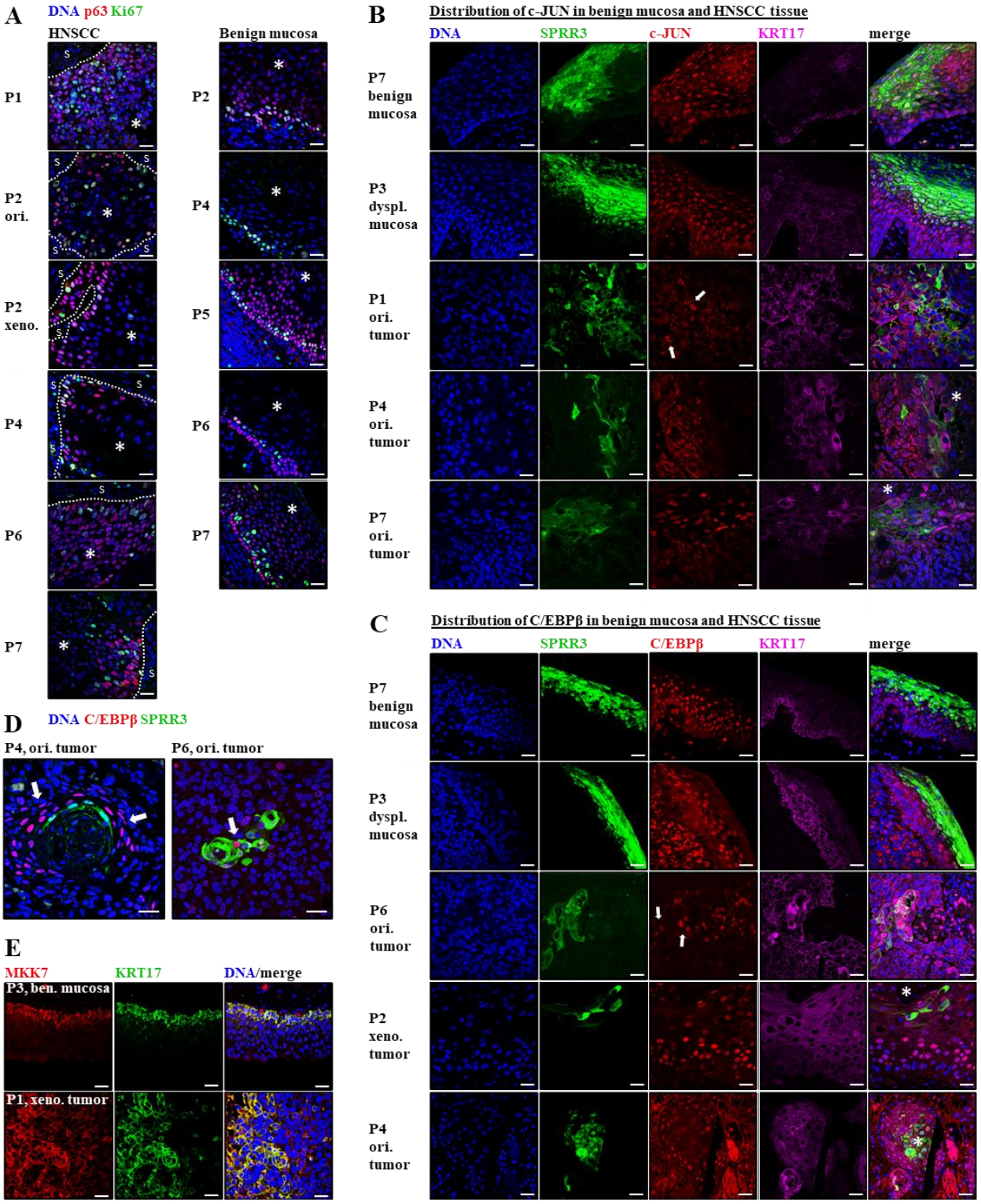
A
DNA p63 Ki67
HNSCC
Benign mucosa
P1
P2
P2 ori.
P4
P2 xeno.
P5
P4
P6
P6
P7
P7
B
Distribution of c-JUN in benign mucosa and HNSCC tissue
DNA
SPRR3
c-JUN
KRT17
merge
P7 benign mucosa
P3 dyspl. mucosa
P1 ori. tumor
P4 ori. tumor
P7 ori. tumor
C
Distribution of C/EBPβ in benign mucosa and HNSCC tissue
DNA
SPRR3
C/EBPβ
KRT17
merge
P7 benign mucosa
P3 dyspl. mucosa
P6 ori. tumor
P2 xeno. tumor
P4 ori. tumor
D
DNA C/EBPβ SPRR3
P4, ori. tumor
P6, ori. tumor
E
MKK7
KRT17
DNA/merge
P3, ben. mucosa
P1, xeno. tumor

Figure 7

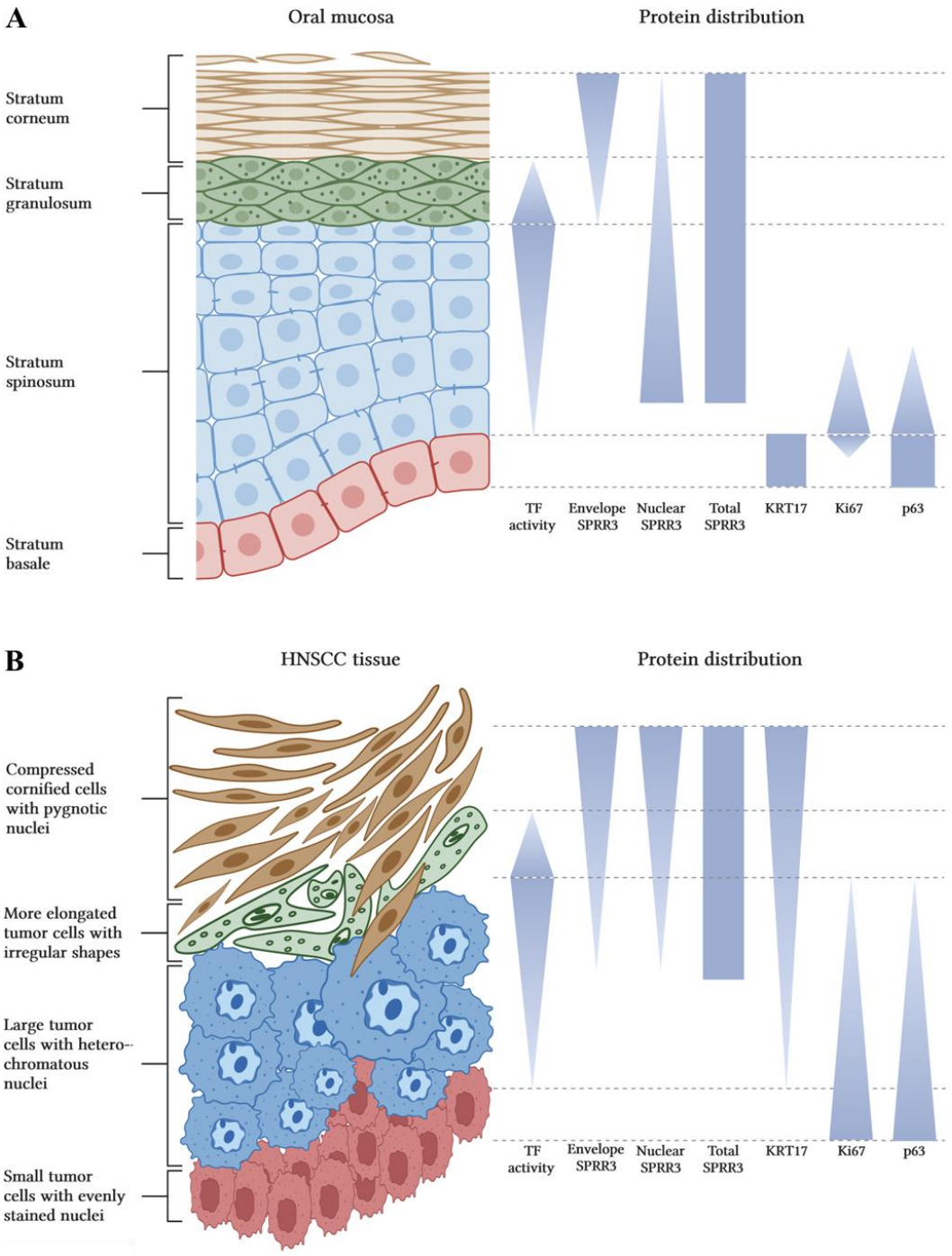
A
Oral mucosa
Protein distribution
Stratum corneum
Stratum granulosum
Stratum spinosum
Stratum basale
TF activity
Envelope SPRR3
Nuclear SPRR3
Total SPRR3
KRT17
Ki67
p63
B
HNSCC tissue
Protein distribution
Compressed cornified cells with pygnotic nuclei
More elongated tumor cells with irregular shapes
Large tumor cells with hetero-chromatous nuclei
Small tumor cells with evenly stained nuclei
TF activity
Envelope SPRR3
Nuclear SPRR3
Total SPRR3
KRT17
Ki67
p63

Figure Legends

Figure 1: HNSCC differentiation can be modeled diminishing cell malignancy. (A) Cells of P1 grow as spheroids in SCM, whereas P2 cultures display a loosely adherent cell layer that forms spheroids and releases them into the culture medium. Treatment of SCM cultures with differentiation medium (CFM) results in the formation of an adherent layer of enlarged cells with irregular shapes. P1 cells show in CFM show cell inclusions and bubble-like structures reminiscent of cornification. **(B)** CFM-treated cells of P1 lose proliferation, whereas cells of P2 continue to expand. **(C)** Cornification assay reveals cornified envelope formation in P1-derived CFM-treated cells, which was not observed for P2; *p = 0.0005; ns = not significant; determined by student`s t-test. **(D)** Single-cell cloning assay for 21 days (d21) confirms efficient self-renewal and clonal re-population capacity of SCM-grown spheroid cells of P1 which was totally abolished in CFM. Adherent and spheroid cells of P2 in SCM were equally able to form spheroids from single cells. Spheroid cells in SCM showed a reduced but not diminished tendency to form adherent colonies from single cells. Single cells of P2 in CFM did not form spheroids but only adherent colonies; *p < 0.05; **p < 0.01; ***p < 0.005; ****p < 0.0001; ns = not significant, determined by student`s t-test. **(E)** Examples for representative clonal cultures at day 21 (d21) derived from **(D)**. **(F)** Treatment with differentiation medium for 21 days reduces the survival of single cell clones of P1 and P2; *p < 0.05; **p < 0.01; ***p < 0.001; ns = not significant, determined by student`s t-test. **(G)** Subcutaneous transplantation of undifferentiated (SCM) and differentiated (CFM) populations into immunodeficient NSG mice showed abolished tumor-initiating cell potential of CFM-treated cells of P1. In P2, CFM significantly reduced TIC capacity. No significant differences were observed between adherent and spheroid cells within the SCM population; *p < 0.05; **p < 0.005; ***p < 0.0005, determined by student`s t-test at the end point of the experiment.

Figure 2: Integration of ATAC-seq, RNA-seq, and Nano-LC-ESI MS/MS identifies differentiation-associated signaling in HNSCC cells. (A) Schematic of the next-generation sequencing and mass-spectrometry approaches to identify the changes underlying tumor cell cornification in HNSCC. **(B)** Genomic annotation of the OCRs in the cancer cells from both HNSCC patients showed a decrease in accessible areas upon differentiation (**p < 0.01). **(C)** Although, the proportion of small open promoters (<1kb) increased with technical replicates (n=3) and a statistical cut-off q-value of 0.05 for peak calling. **(D)** GO terms display the relevant signaling pathways linked to the differential called OCRs within the differentiated cancer cells of both patients with Fisher's exact test. **(E)** Advanced global expression comparison between patients, showing significant transcriptome changes with hundreds to thousands of differentially expressed transcripts regarding the sensitivities towards tumor differentiation and cornification with technical replicates (n=3, except P1 undifferentiated n=2) and a statistical cut-off p-value of 0.05. **(F)** Advanced comparison between the less sensitive and the highly sensitive cultures made it possible to investigate the seemingly essential differences for the cancer cells to differentiate and keratinize. GOs demonstrate negative and positive correlating pathways making P2 the less sensitive culture.

Figure 3: Footprinting, global expression, and proteome analyses identified distinct regulators of the differentiation mechanism in HNSCC. (A) Relevant pathways of HNSCC differentiation are Keratinization, IL6-JAK/STAT3, and TGF-β signaling, identified by gene ontology motif analysis (GOMo) and GSEA. **(B)** Transcription factor footprinting identified p63, c-JUN, C/EBPβ, and SMAD2/3 motifs in differentiating cancer cells. **(C)** KRT17 was only accessible in highly sensitive cultures. **(D**) RNA-seq identified 24 upregulated and 23 downregulated kinases upon differentiation in P1. Regarding P2, 10 kinases were upregulated, and 13 were downregulated. **(E)** The global proteome analysis revealed kinases present during the differentiation of HNSCC cultures from three different time points. The proteome was substituted from the control culture showing kinases only present in the differentiated condition.

Kinases identified in both patients' proteomes are highlighted in orange. **(F)** The Reactome of the global kinase profile emphasizes the similarities and differences regarding the signaling pathways of highly and less differentiation-sensitive cancer cells of P1 and P2 upon treatment with differentiation medium. Kinases overlapping between P1 and P2 are highlighted in orange.

Figure 4: KRT17 expression indicates differentiation in HNSCCs. (A) P1 cells upregulate KRT17 and late cornification marker SPRR3 upon treatment with differentiation medium (CFM) while undifferentiated spheroid cells in stem cell medium (SCM) stain negative for this marker. In P2, KRT17 expression is restricted to a subpopulation in both media which was also observed in adherent (adh.) and spheroid (sph.) cells in SCM. **(B)** KRT17 was strongly expressed around SPRR3+ patches in the original patient`s HNSCC tissue and xenograft tumors in immunodeficient mice of P1 and P2, but not in normal mucosa of those patients. KRT17 seems to precede SPRR3 expression in human HNSCC tissue. **(C)** The tumor-specific association of KRT17 and cornification indicated by SPRR3 was reproduced in four additional patients (P3-P6). In benign mucosa of the same individuals KRT17 was barely visible in the basal layer only or not detectable, when imaged using the same instrument settings as used for the tumor sections. **(D)** Dysplastic mucosa attached to the tumor tissue of P2 and P3 showed a more abundant expression of KRT17 compared to normal mucosa spreading from the basal layer into the SPRR3+ zone; staining by indirect immunofluorescence (IF); scale bars = 10 µm.

Figure 5: Inflammatory cytokines trigger differentiation of HNSCC cells. (A) HNSCC tissue shows cornified cells at the interface between vital tumor tissue and necrotic/immune cell-infiltrated areas and dead cornified cells in the necrotic cavity (arrows); scale bars = 50 µm. **(B)** IF analysis confirms the upregulation of cornification marker SPRR3 at the edge of necrotic/immune cell-infiltrated areas; scale bars = 10µm. **(C)** Treatment of undifferentiated HNSCC cells with combinations of inflammatory cytokines results in cell adhesion, activation of signaling through phosphor-STAT3-Y705 (pSTAT3), and upregulation of differentiation marker KRT17 and cornification marker SPRR3 compared to the untreated control (Con.). Single cytokines like IL19 and OSM were able to induce this differentiation phenotype, but higher numbers of cytokines in combination worked increasing effective; cytokine mix (CK Mix) = EGF, IL1α, IL1β, IL6, IL17A, IL22, TGFβ, OSM, and TNFα. Cells were treated for 5 days in SCM without hydrocortisone; cytokine concentration = 30 ng/ml; scale bars phase contrast = 200 µm; scale bars IF = 10 µm. **(D)** RT-qPCR shows increased relative expression of adhesion marker ITGB1, KRT17, and SPRR3 compared to the untreated control. Cells were treated with CK Mix for 3 days in SCM without hydrocortisone; cytokine concentration = 30 ng/ml; *$p < 0.01$; **$p < 0.005$; ***$p < 0.0001$, determined by student`s t-test.

Figure 6: HNSCC differentiation resembles benign mucosa in tissue architecture. (A) Basal cell marker p63 (21) and proliferation marker colocalize in benign and malignant tissue detected by IF. In benign mucosa, nuclear p63 is observed in the basal layer and in the lower stratum spinosum with Ki67+ cells located in a small layer above the basal cells. In HNSCC, a zone of cells positive for p63 and/or Ki67 is located at the tumor-stroma interface (dashed line, S = stroma) and both markers are downregulated towards the area of tumor differentiation (indicated by *). For example, P1 tumor tissue is poorly organized, largely undifferentiated, and shows abundant p63 and Ki67 expression which decreases only surrounding a necrotic area. In contrast, HNSCCs of P2 and P4 show higher differentiation and contain only a small layer of p63 and Ki67 expressing cells. **(B-C)** HNSCC activates signaling via transcription factors c-JUN **(B)** and C/EBPβ **(C).** Representative examples are shown: each two benign mucosa (normal/dysplastic) samples, one poorly organized differentiating HNSCC (P1 or P6), and two higher organized differentiating HNSCCs (P2 and P4 or P4 and P7). Highly organized tumors and benign mucosa display a layer of cells with nuclear c-JUN and C/EBPβ right above the p63/Ki67+ layer detected in **(A)**. In these samples, basal cells in benign tissue and cells at the

tumor-stroma interface in HNSCC show cytoplasmic location of these markers. Poorly organized tumors show fewer nuclear c-JUN/C/EBPβ+ cells (arrows) which were mixed in between the SPRR3+ differentiated tumor cells indicating a perturbated layer organization. **(D)** Large (P4) and small (P6) areas of cornification harbor a zone of active signaling close to or within the SPRR3+ zone (indicated by nuclear C/EBPβ, arrows). **(E)** Increased MKK7 (MEK-7) expression colocalizes with increased KRT17 signal intensity in normal mucosa of P3 and in xenograft tumor tissue of P1. Xenograft tumor tissue in immunodeficient mice = xeno. tumor; ori. tumor = original tumor tissue; dyspl. = dysplastic; scale bars = 10 µm.

Figure 7: Tissue architecture of oral mucosa and HNSCC. Schematic visualization of cell layer organization in **(A)** normal oral mucosa and **(B)** differentiated areas of HNSCC tissue. Protein marker distribution of KRT17, SPRR3, p63, proliferation marker Ki67 and transcription factors (TF) of the active signaling zone (e.g. C/EBPβ and c-JUN) is depicted. Please note that tumor tissue varies strongly in the proportional representation of each displayed layer. Created with Biorender.com.

Acknowledgments

The authors thank Thorsten Seidel and the imaging facility of the Faculty for Biology of Bielefeld University for their support of this study.

The authors acknowledge the technical NGS team of the Omics CF NGS Unit and CeBiTec.

Funding

This project was funded by the 3-year head and neck cancer program of the Medical Faculty OWL at Bielefeld University.

Ministerio de Ciencia e Innovación/AEI: Agencia Estatal de Investigación/ 10.13039/501100011033/ y financiado por la Unión Europea “NextGenerationEU”/ PRTR (PID2020-115112RB-I00)

Author contributions

Conceptualization, F.O.; methodology, F.O., S.G., L.M., K.N., J.K., D.L., and T.B.; validation, F.O., S.G., and L.M.; formal analysis, F.O., S.G., and L.M.; investigation, F.O., S.G., L.M., J.F.,

A.L., L.H., P.K., P.S., H.P., L.L., M.S., F.V.F., J.N., D.L., and F.B.; resources, L.U.S., F.B., G.E. K.N., J.K., T.B., and H.S.; data curation, F.O. and S.G.; software, S.G.; writing—original draft preparation, F.O. and S.G.; writing-review and editing, F.O., S.G., L.M., J.F., A.L., L.H., H.P., L.L., P.K., P.S., F.V.F., J.N., M.S., P.G., L.U.S., D.L., G.E., F.B., K.N., J.K., and T.B., and H.S.; visualization, F.O., S.G., and L.M.; supervision, F.O., S.G., G.E., T.B., K.N., J.K., and H.S.; project administration, F.O., L.U.S., G.E., F.B., T.B., K.N., J.K., and H.S.; funding acquisition, F.O., P.G., G.E. and H.S..

Data and materials availability

All data not contained in this manuscript will be deposited in a publicly accessible database upon acceptance.

Supplementary Materials (see separate document)

Supplementary Figure S1: HNSCC model of patient 2 (P2)

Supplementary Figure S2: Histology analysis of xenograft tumors in immunodeficient mice

Supplementary Figure S3: Analysis of signaling pathway activation in HNSCC cell culture models of P1 and P2

Supplementary Figure S4: Pathways signaling via TGFβ, JNK, and STAT3 are involved in the differentiation of P1 cells

Supplementary Figure S5: Histology of original tumor tissue of patients 3-7

Supplementary Figure S6: HNSCC tissue exhibits differentiation by cornification

Supplementary Table S1: Patient characteristics

Supplementary Table S2: Taq information of the differential peak analysis of the ATAC-seq

Supplementary Table S3: Genome peak distribution of the ATAC-seq from patient 1 and patient 2

Supplementary Table S4: The differential peak analysis of the ATAC-seq of patient 1

Supplementary Table S5: The differential peak analysis of the ATAC-seq of patient 2

Supplementary Table S6: ATAC-seq differential OCRs GO:BP patient 1

Supplementary Table S7: ATAC-seq differential OCRs GO:BP patient 2

Supplementary Table S8: The differential expression analysis of the RNA-seq of patient 1 diff. medium upregulated

Supplementary Table S9: The differential expression analysis of the RNA-seq of patient 1 diff. medium downregulated

Supplementary Table S10: RNA-seq diff. upregulated GO:BP patient 1

Supplementary Table S11: RNA-seq diff. downregulated GO:BP patient 1

Supplementary Table S12: The differential expression analysis of the RNA-seq of patient 2 diff. medium upregulated

Supplementary Table S13: The differential expression analysis of the RNA-seq of patient 2 diff. medium downregulated

Supplementary Table S14: RNA-seq diff. upregulated GO:BP patient 2

Supplementary Table S15: RNA-seq diff. downregulated GO:BP patient 2

Supplementary Table S16: The differential expression analysis of the RNA-seq of patient 2 versus patient 1 upregulated

Supplementary Table S17: The differential expression analysis of the RNA-seq of patient 2 versus patient 1 downregulated

Supplementary Table S18: Global proteome data from day 1 of patient 1 showing kinases only present in differentiated cancer cells

Supplementary Table S19: Global proteome data from day 4 of patient 1 showing kinases only present in differentiated cancer cells

Supplementary Table S20: Global proteome data from day 8 of patient 1 showing kinases only present in differentiated cancer cells

Supplementary Table S21: Global proteome data from day 1 of patient 2 showing kinases only present in differentiated cancer cells

Supplementary Table S22: Global proteome data from day 4 of patient 2 showing kinases only present in differentiated cancer cells

Supplementary Table S23: Global proteome data from day 8 of patient 2 showing kinases only present in differentiated cancer cells

Supplementary Table S24: Reactome of all kinases only present in differentiated cancer cells from patient 1

Supplementary Table S25: Reactome of all kinases only present in differentiated cancer cells from patient 2

Supplementary Methods

Supplementary References

References

1. Bray F, Ferlay J, Soerjomataram I, Siegel RL, Torre LA, Jemal A. Global cancer statistics 2018: GLOBOCAN estimates of incidence and mortality worldwide for 36 cancers in 185 countries. CA: a cancer journal for clinicians **2018**;68:394-424

2. Ferlay J, Colombet M, Soerjomataram I, Mathers C, Parkin DM, Pineros M*, et al.* Estimating the global cancer incidence and mortality in 2018: GLOBOCAN sources and methods. International journal of cancer **2019**;144:1941-53

3. Johnson DE, Burtness B, Leemans CR, Lui VWY, Bauman JE, Grandis JR. Head and neck squamous cell carcinoma. Nature reviews Disease primers **2020**;6:92

4. Denecker G, Ovaere P, Vandenabeele P, Declercq W. Caspase-14 reveals its secrets. The Journal of cell biology **2008**;180:451-8

5. Candi E, Schmidt R, Melino G. The cornified envelope: a model of cell death in the skin. Nature reviews Molecular cell biology **2005**;6:328-40

6. Enane FO, Saunthararajah Y, Korc M. Differentiation therapy and the mechanisms that terminate cancer cell proliferation without harming normal cells. Cell death & disease **2018**;9:912

7. Lawson DA, Kessenbrock K, Davis RT, Pervolarakis N, Werb Z. Tumour heterogeneity and metastasis at single-cell resolution. Nature cell biology **2018**;20:1349-60

8. Fujii M, Sato T. Defining the role of Lgr5(+) stem cells in colorectal cancer: from basic research to clinical applications. Genome medicine **2017**;9:66

9. Ball CR, Oppel F, Ehrenberg KR, Dubash TD, Dieter SM, Hoffmann CM*, et al.* Succession of transiently active tumor-initiating cell clones in human pancreatic cancer xenografts. EMBO molecular medicine **2017**;9:918-32

10. Dubash TD, Hoffmann CM, Oppel F, Giessler KM, Weber S, Dieter SM*, et al.* Phenotypic differentiation does not affect tumorigenicity of primary human colon cancer initiating cells. Cancer letters **2016**;371:326-33

11. Oppel F, Shao S, Schurmann M, Goon P, Albers AE, Sudhoff H. An Effective Primary Head and Neck Squamous Cell Carcinoma In Vitro Model. Cells **2019**;8

12. Lee J, Kotliarova S, Kotliarov Y, Li A, Su Q, Donin NM*, et al.* Tumor stem cells derived from glioblastomas cultured in bFGF and EGF more closely mirror the phenotype and genotype of primary tumors than do serum-cultured cell lines. Cancer cell **2006**;9:391-403

13. van den Ameele J, Krautz R, Cheetham SW, Donovan APA, Llora-Batlle O, Yakob R*, et al.* Reduced chromatin accessibility correlates with resistance to Notch activation. Nature communications **2022**;13:2210

14. Blanco MA, Sykes DB, Gu L, Wu M, Petroni R, Karnik R*, et al.* Chromatin-state barriers enforce an irreversible mammalian cell fate decision. Cell reports **2021**;37:109967

15. Aughey GN, Estacio Gomez A, Thomson J, Yin H, Southall TD. CATaDa reveals global remodelling of chromatin accessibility during stem cell differentiation in vivo. eLife **2018**;7

16. Dai L, Aye Thu C, Liu XY, Xi J, Cheung PC. TAK1, more than just innate immunity. IUBMB life **2012**;64:825-34

17. Kitamura R, Toyoshima T, Tanaka H, Kawano S, Kiyosue T, Matsubara R*, et al.* Association of cytokeratin 17 expression with differentiation in oral squamous cell carcinoma. Journal of cancer research and clinical oncology **2012**;138:1299-310

18. Zhang X, Yin M, Zhang LJ. Keratin 6, 16 and 17-Critical Barrier Alarmin Molecules in Skin Wounds and Psoriasis. Cells **2019**;8

19. Mokhtari S. Mechanisms of cyst formation in metastatic lymph nodes of head and neck squamous cell carcinoma. Diagnostic pathology **2012**;7:6

20. Hanel KH, Cornelissen C, Luscher B, Baron JM. Cytokines and the skin barrier. International journal of molecular sciences **2013**;14:6720-45

21. Truong AB, Kretz M, Ridky TW, Kimmel R, Khavari PA. p63 regulates proliferation and differentiation of developmentally mature keratinocytes. Genes & development **2006**;20:3185-97

22. Shu H, Wildhaber T, Siretskiy A, Gruissem W, Hennig L. Distinct modes of DNA accessibility in plant chromatin. Nature communications **2012**;3:1281

23. Gaspar-Maia A, Alajem A, Meshorer E, Ramalho-Santos M. Open chromatin in pluripotency and reprogramming. Nature reviews Molecular cell biology **2011**;12:36-47

24. Zimmerman MW, Durbin AD, He S, Oppel F, Shi H, Tao T*, et al.* Retinoic acid rewires the adrenergic core regulatory circuitry of childhood neuroblastoma. Science advances **2021**;7:eabe0834

25. French R, Pauklin S. Epigenetic regulation of cancer stem cell formation and maintenance. International journal of cancer **2021**;148:2884-97

26. Bohmann D, Bos TJ, Admon A, Nishimura T, Vogt PK, Tjian R. Human proto-oncogene c-jun encodes a DNA binding protein with structural and functional properties of transcription factor AP-1. Science **1987**;238:1386-92

27. Maki Y, Bos TJ, Davis C, Starbuck M, Vogt PK. Avian sarcoma virus 17 carries the jun oncogene. Proceedings of the National Academy of Sciences of the United States of America **1987**;84:2848-52

28. Johnson DE, O'Keefe RA, Grandis JR. Targeting the IL-6/JAK/STAT3 signalling axis in cancer. Nature reviews Clinical oncology **2018**;15:234-48

29. Kusaba T, Nakayama T, Yamazumi K, Yakata Y, Yoshizaki A, Inoue K*, et al.* Activation of STAT3 is a marker of poor prognosis in human colorectal cancer. Oncology reports **2006**;15:1445-51

30. Tsushima H, Kawata S, Tamura S, Ito N, Shirai Y, Kiso S*, et al.* High levels of transforming growth factor beta 1 in patients with colorectal cancer: association with disease progression. Gastroenterology **1996**;110:375-82

31. Wikstrom P, Stattin P, Franck-Lissbrant I, Damber JE, Bergh A. Transforming growth factor beta1 is associated with angiogenesis, metastasis, and poor clinical outcome in prostate cancer. The Prostate **1998**;37:19-29

32. Matherne MG, Phillips ES, Embrey SJ, Burke CM, Machado HL. Emerging functions of C/EBPbeta in breast cancer. Frontiers in oncology **2023**;13:1111522

33. Massague J. TGFbeta in Cancer. Cell **2008**;134:215-30

34. Ikushima H, Miyazono K. TGFbeta signalling: a complex web in cancer progression. Nature reviews Cancer **2010**;10:415-24

35. Kuilman T, Michaloglou C, Vredeveld LC, Douma S, van Doorn R, Desmet CJ*, et al.* Oncogene-induced senescence relayed by an interleukin-dependent inflammatory network. Cell **2008**;133:1019-31

36. Acosta JC, O'Loghlen A, Banito A, Guijarro MV, Augert A, Raguz S*, et al.* Chemokine signaling via the CXCR2 receptor reinforces senescence. Cell **2008**;133:1006-18

37. Eferl R, Wagner EF. AP-1: a double-edged sword in tumorigenesis. Nature reviews Cancer **2003**;3:859-68

38. Tolomeo M, Cascio A. The Multifaced Role of STAT3 in Cancer and Its Implication for Anticancer Therapy. International journal of molecular sciences **2021**;22

39. Macha MA, Matta A, Kaur J, Chauhan SS, Thakar A, Shukla NK*, et al.* Prognostic significance of nuclear pSTAT3 in oral cancer. Head & neck **2011**;33:482-9

40. Grandis JR, Drenning SD, Zeng Q, Watkins SC, Melhem MF, Endo S*, et al.* Constitutive activation of Stat3 signaling abrogates apoptosis in squamous cell carcinogenesis in vivo. Proceedings of the National Academy of Sciences of the United States of America **2000**;97:4227-32

41. Huang Q, Ye M, Li F, Lin L, Hu C. Prognostic and clinicopathological significance of transcription factor c-Jun in hypopharyngeal squamous cell carcinoma: a 3-year follow-up retrospective study. BMC cancer **2022**;22:1019

42. Baraks G, Tseng R, Pan CH, Kasliwal S, Leiton CV, Shroyer KR*, et al.* Dissecting the Oncogenic Roles of Keratin 17 in the Hallmarks of Cancer. Cancer research **2022**;82:1159-66

43. Escobar-Hoyos LF, Shah R, Roa-Pena L, Vanner EA, Najafian N, Banach A*, et al.* Keratin-17 Promotes p27KIP1 Nuclear Export and Degradation and Offers Potential Prognostic Utility. Cancer research **2015**;75:3650-62

44. Li C, Su H, Ruan C, Li X. Keratin 17 knockdown suppressed malignancy and cisplatin tolerance of bladder cancer cells, as well as the activation of AKT and ERK pathway. Folia histochemica et cytobiologica **2021**;59:40-8

45. Regenbogen E, Mo M, Romeiser J, Shroyer ALW, Escobar-Hoyos LF, Burke S*, et al.* Elevated expression of keratin 17 in oropharyngeal squamous cell carcinoma is associated with decreased survival. Head & neck **2018**;40:1788-98

46. Tang S, Liu W, Yong L, Liu D, Lin X, Huang Y*, et al.* Reduced Expression of KRT17 Predicts Poor Prognosis in HER2(high) Breast Cancer. Biomolecules **2022**;12

47. Zhang H, Zhang Y, Feng Z, Lu L, Li Y, Liu Y*, et al.* Analysis of the Expression and Role of Keratin 17 in Human Tumors. Frontiers in genetics **2022**;13:801698

48. Qu J, Yi G, Zhou H. p63 cooperates with CTCF to modulate chromatin architecture in skin keratinocytes. Epigenetics & chromatin **2019**;12:31

49. Qu J, Tanis SEJ, Smits JPH, Kouwenhoven EN, Oti M, van den Bogaard EH*, et al.* Mutant p63 Affects Epidermal Cell Identity through Rewiring the Enhancer Landscape. Cell reports **2018**;25:3490-503 e4

50. Kouwenhoven EN, Oti M, Niehues H, van Heeringen SJ, Schalkwijk J, Stunnenberg HG*, et al.* Transcription factor p63 bookmarks and regulates dynamic enhancers during epidermal differentiation. EMBO reports **2015**;16:863-78

51. Soares E, Zhou H. Master regulatory role of p63 in epidermal development and disease. Cellular and molecular life sciences : CMLS **2018**;75:1179-90

52. Yamanaka Y, Nakajima K, Fukada T, Hibi M, Hirano T. Differentiation and growth arrest signals are generated through the cytoplasmic region of gp130 that is essential for Stat3 activation. The EMBO journal **1996**;15:1557-65

53. Nakajima K, Yamanaka Y, Nakae K, Kojima H, Ichiba M, Kiuchi N*, et al.* A central role for Stat3 in IL-6-induced regulation of growth and differentiation in M1 leukemia cells. The EMBO journal **1996**;15:3651-8

54. Shimozaki K, Nakajima K, Hirano T, Nagata S. Involvement of STAT3 in the granulocyte colony-stimulating factor-induced differentiation of myeloid cells. The Journal of biological chemistry **1997**;272:25184-9

55. Dieter SM, Ball CR, Hoffmann CM, Nowrouzi A, Herbst F, Zavidij O*, et al.* Distinct types of tumor-initiating cells form human colon cancer tumors and metastases. Cell stem cell **2011**;9:357-65

56. Clevers H. The intestinal crypt, a prototype stem cell compartment. Cell **2013**;154:274-84

57. Chan CW, Wong NA, Liu Y, Bicknell D, Turley H, Hollins L*, et al.* Gastrointestinal differentiation marker Cytokeratin 20 is regulated by homeobox gene CDX1. Proceedings of the National Academy of Sciences of the United States of America **2009**;106:1936-41

58. Moll R, Schiller DL, Franke WW. Identification of protein IT of the intestinal cytoskeleton as a novel type I cytokeratin with unusual properties and expression patterns. The Journal of cell biology **1990**;111:567-80

59. Merlos-Suarez A, Barriga FM, Jung P, Iglesias M, Cespedes MV, Rossell D*, et al.* The intestinal stem cell signature identifies colorectal cancer stem cells and predicts disease relapse. Cell stem cell **2011**;8:511-24

60. Morris JPt, Cano DA, Sekine S, Wang SC, Hebrok M. Beta-catenin blocks Kras-dependent reprogramming of acini into pancreatic cancer precursor lesions in mice. The Journal of clinical investigation **2010**;120:508-20

61. Shao S, Scholtz LU, Gendreizig S, Martinez-Ruiz L, Florido J, Escames G*, et al.* Primary head and neck cancer cell cultures are susceptible to proliferation of Epstein-Barr virus infected lymphocytes. BMC cancer **2023**;23:47

62. Oppel F, Muller N, Schackert G, Hendruschk S, Martin D, Geiger KD*, et al.* SOX2-RNAi attenuates S-phase entry and induces RhoA-dependent switch to protease-independent amoeboid migration in human glioma cells. Molecular cancer **2011**;10:137

63. Oppel F, Tao T, Shi H, Ross KN, Zimmerman MW, He S*, et al.* Loss of atrx cooperates with p53-deficiency to promote the development of sarcomas and other malignancies. PLoS genetics **2019**;15:e1008039

64. Bray NL, Pimentel H, Melsted P, Pachter L. Near-optimal probabilistic RNA-seq quantification. Nature biotechnology **2016**;34:525-7

65. McCarthy DJ, Chen Y, Smyth GK. Differential expression analysis of multifactor RNA-Seq experiments with respect to biological variation. Nucleic acids research **2012**;40:4288-97

66. Ashburner M, Ball CA, Blake JA, Botstein D, Butler H, Cherry JM*, et al.* Gene ontology: tool for the unification of biology. The Gene Ontology Consortium. Nature genetics **2000**;25:25-9

67. Gene Ontology C. The Gene Ontology resource: enriching a GOld mine. Nucleic acids research **2021**;49:D325-D34

68. Mi H, Muruganujan A, Ebert D, Huang X, Thomas PD. PANTHER version 14: more genomes, a new PANTHER GO-slim and improvements in enrichment analysis tools. Nucleic acids research **2019**;47:D419-D26

69. Subramanian A, Tamayo P, Mootha VK, Mukherjee S, Ebert BL, Gillette MA*, et al.* Gene set enrichment analysis: a knowledge-based approach for interpreting genome-wide expression profiles. Proceedings of the National Academy of Sciences of the United States of America **2005**;102:15545-50

70. Mootha VK, Lindgren CM, Eriksson KF, Subramanian A, Sihag S, Lehar J*, et al.* PGC-1alpha-responsive genes involved in oxidative phosphorylation are coordinately downregulated in human diabetes. Nature genetics **2003**;34:267-73

71. Shannon P, Markiel A, Ozier O, Baliga NS, Wang JT, Ramage D*, et al.* Cytoscape: a software environment for integrated models of biomolecular interaction networks. Genome research **2003**;13:2498-504

72. Buenrostro JD, Wu B, Chang HY, Greenleaf WJ. ATAC-seq: A Method for Assaying Chromatin Accessibility Genome-Wide. Current protocols in molecular biology **2015**;109:21 9 1- 9 9

73. Langmead B, Salzberg SL. Fast gapped-read alignment with Bowtie 2. Nature methods **2012**;9:357-9

74. Li H, Handsaker B, Wysoker A, Fennell T, Ruan J, Homer N*, et al.* The Sequence Alignment/Map format and SAMtools. Bioinformatics **2009**;25:2078-9

75. Zhang Y, Liu T, Meyer CA, Eeckhoute J, Johnson DS, Bernstein BE*, et al.* Model-based analysis of ChIP-Seq (MACS). Genome biology **2008**;9:R137

76. Quinlan AR, Hall IM. BEDTools: a flexible suite of utilities for comparing genomic features. Bioinformatics **2010**;26:841-2

77. Lawrence M, Huber W, Pages H, Aboyoun P, Carlson M, Gentleman R*, et al.* Software for computing and annotating genomic ranges. PLoS computational biology **2013**;9:e1003118

78. Bailey TL, Johnson J, Grant CE, Noble WS. The MEME Suite. Nucleic acids research **2015**;43:W39-49

79. Buske FA, Boden M, Bauer DC, Bailey TL. Assigning roles to DNA regulatory motifs using comparative genomics. Bioinformatics **2010**;26:860-6

80. Heinz S, Benner C, Spann N, Bertolino E, Lin YC, Laslo P*, et al.* Simple combinations of lineage-determining transcription factors prime cis-regulatory elements required for macrophage and B cell identities. Molecular cell **2010**;38:576-89

81. Yu G, Wang LG, He QY. ChIPseeker: an R/Bioconductor package for ChIP peak annotation, comparison and visualization. Bioinformatics **2015**;31:2382-3

82. Wang Q, Li M, Wu T, Zhan L, Li L, Chen M*, et al.* Exploring Epigenomic Datasets by ChIPseeker. Current protocols **2022**;2:e585

83. Jarnik M, Simon MN, Steven AC. Cornified cell envelope assembly: a model based on electron microscopic determinations of thickness and projected density. Journal of cell science **1998**;111 (Pt 8):1051-60